

The second-order formulation of the P_N equations with Marshak boundary conditions

Matthias Andres¹, Florian Schneider²

Abstract

We consider a reformulation of the classical P_N method with Marshak boundary conditions for the approximation of the monoenergetic stationary linear transport equation as a system of second-order PDEs. Our derivation allows the automatic generation of a model hierarchy which can then be handed to standard PDE tools. This method allows for heterogeneous coefficients, irregular grids, anisotropic boundary sources and anisotropic scattering. The wide applicability is demonstrated in several numerical test cases. We make our implementation available online, which allows for fast prototyping.

Keywords: moment models, kinetic transport equation, automatic model generation

2010 MSC: 35L40, 35Q70, 65M60, 65M70

1. Introduction

This article is intended to provide a straight-forward derivation of a hierarchy of approximate models for the monoenergetic stationary linear transfer equation (msLTE) based on the P_N equations with Marshak boundary conditions. The method is designed to be applicable in a general set of situations, e.g., irregular grids in up to three spatial dimensions, heterogeneous coefficients, anisotropic scattering or anisotropic boundary sources. We provide a demo implementation in MATLAB and PYTHON, which allows for fast prototyping.

This equation appears as a model for photon radiation transport in various physical applications, e.g., radiation transport in biological tissue during certain cancer therapies [1] or in high-temperature processes in industry [2].

Due to the dependence on up to three space variables and two directional variables it is hard to solve the msLTE directly. One common way to discretize the solution is the P_N method, e.g., [3], a type of spectral approximation in the directional variable, which results in a system of first-order partial differential equations in space. The numerical treatment of the resulting system of equations is described for the time-dependent case on a staggered grid in [4].

Another way of approximation are *Simplified* P_N (SP_N) methods, which can be derived in different ways from the P_N equations. All of them have the common goal to derive a smaller system of second-order partial differential equations in space, which then can be solved by standard PDE tools, e.g., [5]. As mentioned in [6], the second-order formulation has less unknowns and does not require additional stabilization for the price of the generated matrix being less sparse. A review on different ways to derive SP_N equations is given in [7]. The described SP_N models are under certain assumptions equivalent to the corresponding SP_N models and numerical results suggested that the SP_N models give higher-order corrections to the diffusion approximation of the msLTE [7].

We follow the same approach as in [8–10]. We take a subset of the P_N equations to express the odd moments in terms of even moments by algebraic transformations. We plug the resulting terms into the

¹Fachbereich Mathematik, TU Kaiserslautern, Erwin-Schrödinger-Str., 67663 Kaiserslautern, Germany, andres@mathematik.uni-kl.de

²Fachbereich Mathematik, TU Kaiserslautern, Erwin-Schrödinger-Str., 67663 Kaiserslautern, Germany, schneider@mathematik.uni-kl.de

remaining equations and by this transform the system of first-order PDEs into a system of second-order PDEs. This is different from the classical ad-hoc SP_N derivation in 1D slab geometry, e.g., [11–15], as we perform all calculations on the full 3D system. One advantage of this, depending on a few mild assumptions on the coefficients and the regularity of the solutions, is the equivalence of the solutions to those of the original P_N method what is discussed as one of the main issues of the classical SP_N approach [16]. This approach comes along with two issues that we would like to address in this work. First, the algebraic transformations become very tedious and result in lengthy expressions. Second, there is an ambiguity of choosing the “relevant” subset of half-moments for the Marshak boundary conditions.

By choosing a suitable formulation of the P_N system we are able to delegate the transformation to a computer algebra system (e.g., MATLAB’s Symbolic Toolbox [17]) and thus automatize the tedious algebraic calculations. The result can be forwarded to a standard PDE tool, like done in this work to the PYTHON Toolbox FEniCS [18, 19]. Furthermore we suggest a certain selection of boundary half-moments for which we prove the existence of a weak formulation of the second-order system. Here we would like to note that the proper treatment of boundary conditions has been seen as one of the major issues in this context in [16].

Classical SP_N methods produce a system of equations of size $\sim N$, whereas the P_N method as well as our approach yields systems of size $\sim N^2$. Furthermore, eventhough our approach looks similar to the above mentioned ad-hoc derivation, it does not yield a “simplified” version of the P_N equations, but an equivalent “second-order” formulation, provided that the P_N solution is smooth enough to allow all steps during the transformation. We will refer to our method as $P_N^{2\text{nd}}$.

Similar to [4, 20], we follow the FAIR guiding principles for scientific research [21] and make all codes, including files to generate the numerical results of this article, available to the reader online [22].

In Section 2 we review the standard P_N approach, which is then reformulated as a system of second-order PDEs in space in Section 3. In Section 4 we look at different examples in one and two space dimensions to demonstrate the wide applicability of our approach, followed by concluding remarks in Section 5.

2. Modeling

We consider the monoenergetic stationary linear transport equation, e.g., [23],

$$\boldsymbol{\Omega} \cdot \nabla_{\mathbf{x}} I + \sigma_a I = \sigma_s \mathcal{C}(I), \quad (1)$$

which describes the time-stationary density of particles at **position** $\mathbf{x} = (x, y, z)^T$ in a domain $X \subseteq \mathbb{R}^3$ with speed $\boldsymbol{\Omega} \in \mathcal{S}^2 = \{\boldsymbol{\Omega} \in \mathbb{R}^3 : \|\boldsymbol{\Omega}\|_2 = 1\}$ under the events of **scattering** (proportional to $\sigma_s(\mathbf{x})$) and **absorption** (proportional to $\sigma_a(\mathbf{x})$). The quantity $\sigma_t := \sigma_a + \sigma_s$ is called the **attenuation** coefficient.

Collisions are modeled using the BGK-type collision [24, 25] operator

$$\mathcal{C}(I) = \int_{\mathcal{S}^2} \kappa(\boldsymbol{\Omega}, \boldsymbol{\Omega}') I(\mathbf{x}, \boldsymbol{\Omega}') d\boldsymbol{\Omega}' - \int_{\mathcal{S}^2} \kappa(\boldsymbol{\Omega}', \boldsymbol{\Omega}) I(\mathbf{x}, \boldsymbol{\Omega}) d\boldsymbol{\Omega}', \quad (2)$$

with collision kernel $\kappa : \mathcal{S}^2 \times \mathcal{S}^2 \rightarrow \mathbb{R}$.

Assumption 2.1. *We assume the collision kernel κ to be:*

(A1) *Strictly positive:* $\kappa(\boldsymbol{\Omega}, \boldsymbol{\Omega}') \geq \kappa_0 > 0$ for all $\boldsymbol{\Omega}, \boldsymbol{\Omega}' \in \mathcal{S}^2$;

(A2) *Symmetric:* $\kappa(\boldsymbol{\Omega}, \boldsymbol{\Omega}') = \kappa(\boldsymbol{\Omega}', \boldsymbol{\Omega})$ for all $\boldsymbol{\Omega}, \boldsymbol{\Omega}' \in \mathcal{S}^2$;

(A3) *Normalized:* $\int_{\mathcal{S}^2} \kappa(\boldsymbol{\Omega}', \boldsymbol{\Omega}) d\boldsymbol{\Omega}' \equiv 1$ for all $\boldsymbol{\Omega} \in \mathcal{S}^2$.

Example 2.2. *Choosing the kernel to be constant, i.e., $\kappa(\boldsymbol{\Omega}, \boldsymbol{\Omega}') \equiv \frac{1}{|\mathcal{S}^2|} = \frac{1}{4\pi}$ for all $\boldsymbol{\Omega}, \boldsymbol{\Omega}' \in \mathcal{S}^2$, yields isotropic scattering.*

Example 2.3. A typical example for anisotropic scattering is the **Henyey-Greenstein** kernel [26]:

$$\kappa(\boldsymbol{\Omega}, \boldsymbol{\Omega}') = \frac{1}{4\pi} \frac{1 - g^2}{\left(1 + g^2 - 2g \cos\left(\boldsymbol{\Omega}^T \boldsymbol{\Omega}'\right)\right)^{\frac{3}{2}}}. \quad (3)$$

The parameter $g \in [-1, 1]$ can be used to blend from backscattering ($g = -1$) over isotropic scattering ($g = 0$) to forward scattering ($g = 1$).

The transport Equation (1) is equipped with semi-transparent boundary conditions, e.g., [27], of the form

$$I(\mathbf{x}, \boldsymbol{\Omega}) = \rho(\mathbf{x}, \boldsymbol{\Omega})I(\mathbf{x}, r(\boldsymbol{\Omega})) + (1 - \rho(\mathbf{x}, \boldsymbol{\Omega}))I_{\Gamma}(\mathbf{x}, \boldsymbol{\Omega}) \quad \text{for } \mathbf{x} \in \Gamma, \mathbf{n}(\mathbf{x}) \cdot \boldsymbol{\Omega} < 0, \quad (4)$$

where $\Gamma := \partial X$ is the boundary of the domain, I_{Γ} is a given boundary distribution, $\rho(\mathbf{x}, \boldsymbol{\Omega}) \in [0, 1]$ is the reflectivity coefficient of the boundary and $r(\boldsymbol{\Omega}) = \boldsymbol{\Omega} - 2(\mathbf{n} \cdot \boldsymbol{\Omega})\mathbf{n}$ is the direction reflected at the plane $\{\boldsymbol{\Omega} \in \mathcal{S}^2 : \mathbf{n} \cdot \boldsymbol{\Omega} = 0\}$, where \mathbf{n} denotes the unit outward-pointing normal vector on the domain's boundary Γ . Note that it is only possible to prescribe boundary data for ingoing particles ($\mathbf{n} \cdot \boldsymbol{\Omega} < 0$) since particles moving in the opposite direction cannot enter the domain.

Remark 2.4. The reflectivity coefficient $\rho(\mathbf{x}, \boldsymbol{\Omega})$ describes the ratio between reflected and transmitted radiation at a point $\mathbf{x} \in \Gamma$ at the boundary. It can be calculated according to Fresnel's equation and Snell's law, e.g., [27] and depends on the refractive indices of the adjacent materials inside and outside of the domain. Furthermore it depends on the inner product $\mathbf{n}(\mathbf{x}) \cdot \boldsymbol{\Omega}$, i.e., on the angle relative to the normal vector. In order to simplify the derivation of the second-order formulation and reduce complex boundary effects in the numerical test cases we drop the directional dependency, i.e., we set $\rho(\mathbf{x}, \boldsymbol{\Omega}) = \rho(\mathbf{x})$. The derivation and implementation can be extended to the direction-dependent case.

Assumption 2.5 (Well posedness of the msLTE). For the following we assume that the parameters are chosen in such a way that the msLTE admits a unique solution.

In many applications, e.g., [1, 2, 28, 29], we are not interested on the directional dependence, but only in the radiative energy of the distribution:

$$\phi(\mathbf{x}) = \int_{\mathcal{S}^2} I(\mathbf{x}, \boldsymbol{\Omega}) \, d\boldsymbol{\Omega}. \quad (5)$$

Throughout this paper we parametrize the direction $\boldsymbol{\Omega}$ in cylindrical coordinates by

$$\boldsymbol{\Omega} = \left(\sqrt{1 - \mu^2} \cos(\varphi), \sqrt{1 - \mu^2} \sin(\varphi), \mu\right)^T =: (\Omega_x, \Omega_y, \Omega_z)^T, \quad (6)$$

where $\varphi \in [0, 2\pi]$ is the azimuthal angle and $\mu \in [-1, 1]$ the cosine of the polar angle. With this we can evaluate the integral over the full sphere \mathcal{S}^2 as follows:

$$\langle \cdot \rangle := \int_{\mathcal{S}^2} \cdot \, d\boldsymbol{\Omega} = \int_{-1}^1 \int_0^{2\pi} \cdot \, d\varphi \, d\mu.$$

2.1. Moment approximations

The following brief overview on moment approximations is based on and adopted in part from [30]. In general, solving Equation (1) numerically is computationally expensive since in three spatial dimensions the state space $X \times \mathcal{S}^2$ of I is a subset of \mathbb{R}^5 .

For this reason it is convenient to use some type of spectral or Galerkin method to transform the high-dimensional equation into a system of lower-dimensional equations. Typically, one chooses to reduce the dimensionality by representing the angular dependency of I in terms of some angular basis, where in this paper we choose the so-called **real spherical harmonics** with maximum degree N .

Definition 2.6. The real spherical harmonics [4, 31, 32] can be obtained from the complex spherical harmonics [33, §VII.5]

$$Y_l^m(\mu, \varphi) = (-1)^m \cdot \underbrace{\sqrt{\frac{(2l+1)(l-m)!}{4\pi(l+m)!}}}_{=: \Theta_{lm}(\mu)} P_l^m(\mu) \cdot e^{im\varphi} \quad (7)$$

with $0 \leq l \leq N$, $-l \leq m \leq l$, by splitting them into real and imaginary part [32], i.e.,

$$S_l^m(\mu, \varphi) = \begin{cases} \Theta_{lm}(\mu)\sqrt{2}\cos(m\varphi) & , m > 0, \\ \Theta_{l0}(\mu) & , m = 0, \\ \Theta_{l|m|}(\mu)\sqrt{2}\sin(|m|\varphi) & , m < 0, \end{cases} \quad (8)$$

with Θ_{lm} defined as in Equation (7). Analogous to [32] the associated Legendre polynomials P_l^m are chosen to satisfy the Rodrigues' formula³

$$P_l^m(\mu) = \frac{1}{2^l l!} (1 - \mu^2)^{\frac{m}{2}} \frac{d^{l+m}}{d\mu^{l+m}} (\mu^2 - 1)^l.$$

Here l denotes the **degree** of the corresponding function.

Definition 2.7. Depending on certain symmetry assumptions as discussed in Subsection 2.2 we collect a subset of n real spherical harmonics with maximum degree N in the vector $\mathbf{b} := \mathbf{b}_N : \mathcal{S}^2 \rightarrow \mathbb{R}^n$. In the following we refer to this vector as (angular) basis of order N .

The so-called moments of a given distribution function I are then defined by

$$\mathbf{u} := \mathbf{u}_{\mathbf{b}} := \langle \mathbf{b} I \rangle = \int_{\mathcal{S}^2} \mathbf{b}(\Omega) I(\mathbf{x}, \Omega) d\Omega = (u_0, \dots, u_{n-1})^T, \quad (9)$$

where the integration is performed componentwise.

The set of all real spherical harmonics forms an orthonormal basis of $L_2(\mathcal{S}^2, \mathbb{R})$ [32], what especially implies $\langle \mathbf{b}_i \mathbf{b}_j \rangle = \delta_{i,j}$. This allows to express the distribution I in terms of a Fourier series

$$I(\mathbf{x}, \Omega) = \sum_{i=0}^{\infty} \langle b_i I \rangle b_i = \sum_{i=0}^{\infty} u_i b_i = \mathbf{b}_{\infty} \cdot \mathbf{u}_{\infty}.$$

In order to obtain a set of equations for \mathbf{u} , we perform a Galerkin approximation of Equation (1) by projecting it onto the space spanned by \mathbf{b} . We thus obtain

$$\langle \mathbf{b} \nabla_{\mathbf{x}} \cdot \Omega I \rangle + \langle \mathbf{b} \sigma_a I \rangle = \langle \mathbf{b} \sigma_s \mathcal{C}(I) \rangle. \quad (10)$$

Since it is impractical to work with an infinite-dimensional system, the Fourier series has to be truncated, such that a finite number of $n < \infty$ basis functions \mathbf{b}_N of order N remains. As the real spherical harmonics are orthonormal w.r.t. $\langle \cdot \rangle$ we can choose the ansatz

$$I(\mathbf{x}, \Omega) \approx \hat{I}_{\mathbf{u}}(\mathbf{x}, \Omega) = \sum_{i=0}^{n-1} u_i b_i(\Omega) = \mathbf{b}(\Omega)^T \mathbf{u}. \quad (11)$$

Collecting known terms and interchanging integrals and differentiation where possible, the moment system has the form

$$\langle \Omega_x \mathbf{b} \mathbf{b}^T \rangle \cdot \partial_x \mathbf{u} + \langle \Omega_y \mathbf{b} \mathbf{b}^T \rangle \cdot \partial_y \mathbf{u} + \langle \Omega_z \mathbf{b} \mathbf{b}^T \rangle \cdot \partial_z \mathbf{u} + \sigma_a \mathbf{u} = \sigma_s \langle \mathbf{b} \mathcal{C}(I) \rangle. \quad (12)$$

³Note that sometimes the associated Legendre Polynomials are defined with a prefactor of $(-1)^m$.

By the choice of our basis the first moment $u_0 \approx \left\langle \frac{1}{\sqrt{4\pi}} I \right\rangle = \frac{1}{\sqrt{4\pi}} \phi$ is an approximation of a multiple of the radiative energy defined in Equation (5).

Our choice of the scattering operator and the assumptions on the scattering kernel allow us to write

$$\langle \mathbf{bC}(I) \rangle = (\Sigma - E_n) \mathbf{u}, \quad \text{where } \Sigma = \int_{\mathbb{S}^2} \int_{\mathbb{S}^2} \mathbf{b}(\boldsymbol{\Omega}) \mathbf{b}(\boldsymbol{\Omega}')^T \kappa(\boldsymbol{\Omega}, \boldsymbol{\Omega}') \, d\boldsymbol{\Omega}' \, d\boldsymbol{\Omega}$$

and E_n denotes the $n \times n$ identity matrix.

Remark 2.8. Unfortunately, there always exists an index $i \in \{0, \dots, n-1\}$ in Equation (10) such that the components of $\mathbf{b}_i \boldsymbol{\Omega}$ are not in the linear span of \mathbf{b}_N . Therefore, the flux term cannot be expressed in terms of $\mathbf{u}_{\mathbf{b}_N}$ without additional information. Furthermore, the same might be true for the projection of the scattering operator onto the moment-space given by $\langle \mathbf{bC}(I) \rangle$. This is the so-called closure problem. There exist many different closure strategies related to different types of bases and ansatz functions. Our choice corresponds to the well-known spherical harmonics P_N -model [34, 35], which can be understood as a Galerkin semi-approximation in $\boldsymbol{\Omega}$ for Equation (1).

Remark 2.9. A big disadvantage of this model is the missing positivity of the ansatz-function $\hat{I}_{\mathbf{u}}$ for some moments \mathbf{u} whereas the kinetic distribution to be approximated fulfills this property. Another undesired issue, which is a general problem of unlimited high-order approximations, are non-physical oscillations where the kinetic solution is non-smooth (the so-called Gibbs phenomenon [36, 37]). Additionally, since the resulting system is linear, it might be necessary to use a high number of moments to ensure a reasonable approximation of the desired kinetic solution. A problem coming along with the linearity of the ansatz is the fact that the resulting wave-speeds of this system are fixed and discrete in contrast to those of the kinetic solution. However, the structure of this system is well-understood and allows for efficient numerical implementations [4, 38].

In recent years many modifications to this closure have been suggested, including the positive P_N (PP_N), filtered P_N (FP_N) and diffusive-corrected P_N (DN) [38], curing some of the disadvantages of the original P_N method while increasing the complexity of the system at the price of higher computational costs. We also want to note that the choices of other closures and angular bases are possible, e.g., minimum entropy [3, 31, 39, 39–49], partial and mixed moments [50–55] or Kershaw closures [56–59].

2.2. Reduction of dimensionality

Due to the computational complexity of Equation (1) it is a common approach to investigate lower-dimensional models. We achieve this by assuming certain symmetries of the solution, implying that it is sufficient to perform the calculations on lower-dimensional spatial slices and a reduced set of basis functions.

- Following [4], “the slab geometry radiative transfer equation is obtained by considering a slab between two infinite parallel plates. Assume for instance that the z -axis is perpendicular to the plates. If the setting is invariant under translations perpendicular to, and rotations around, the z -axis, then the unknown I depends only on the z -component of the spatial variable, and one angular variable μ (cosine of the angle between direction and z -axis)”, i.e., $\partial_x I = \partial_y I = 0$ and $I(\mathbf{x}, \boldsymbol{\Omega}) = I(z, \mu)$. The functions S_l^m with $m = 0$ depend on the azimuthal variable φ and thus do not appear in the series expansion of a distribution I with the assumed symmetry. This allows us to consider the one-dimensional approximation space $X \subset \mathbb{R}$ in space⁴ and define the reduced angular basis

$$\mathbf{b}_N = (S_0^0, S_1^0, \dots, S_N^0).$$

We note that the real spherical harmonics S_l^m with $m = 0$ correspond to the normalized Legendre

⁴Note that the same symbol is used for the one-dimensional projection and for the full space.

polynomials⁵. The P_N equations then read

$$\underbrace{\langle \Omega_z \mathbf{b} \mathbf{b}^T \rangle}_{T_z} \partial_z \mathbf{u} = (\sigma_s \Sigma - \sigma_t E_n) \mathbf{u}. \quad (13)$$

Due to the recursive structure of the Legendre polynomials [4] the flux matrix has the tridiagonal form

$$\left. \begin{aligned} (T_z)_{l,l+1} &= \sqrt{\frac{1}{4l^2 + 8l + 3}} (l + 1) = (T_z)_{l+1,l} \\ (T_z)_{l,l} &= 0 \end{aligned} \right\} \quad \text{for } l = 0, \dots, N.$$

- If the domain is instead assumed to be infinitely elongated in the z -direction and all data is z -independent, the solution I of Equation (1) is also z -independent and even in μ [4], i.e., $\partial_z I = 0$ and $I(\mathbf{x}, \mu, \varphi) = I(\mathbf{x}, -\mu, \varphi)$. The functions S_l^m with $l + |m|$ odd are odd in μ and thus do not appear in the series expansion of the solution. This allows us to consider the (two-dimensional) approximation space $X \subset \mathbb{R}^2$ in space and define the reduced angular basis

$$\mathbf{b}_N = (S_0^0, S_1^{-1}, S_1^1, \dots, S_N^{-N}, S_N^{-N+2}, \dots, S_N^{N-2}, S_N^N)^T,$$

i.e., we use only the subset of the real spherical harmonics where $l + |m|$ is even. The corresponding system then has the form

$$\underbrace{\langle \Omega_x \mathbf{b} \mathbf{b}^T \rangle}_{T_x} \partial_x \mathbf{u} + \underbrace{\langle \Omega_y \mathbf{b} \mathbf{b}^T \rangle}_{T_y} \partial_y \mathbf{u} = (\sigma_s \Sigma - \sigma_t E_n) \mathbf{u}. \quad (14)$$

The matrices T_x, T_y, T_z can be found in [4].

- If we do not assume any symmetry properties of the data and the solution, we include all real spherical harmonics up to degree N in our angular basis:

$$\mathbf{b}_N = (S_0^0, S_1^{-1}, S_1^0, S_1^1, \dots, S_N^{-N}, S_N^{-N+1}, \dots, S_N^{N-1}, S_N^N)^T.$$

Remark 2.10 (Reduced angular bases). *Based on the symmetry assumption described above, some of the basis functions which are necessary in the full three-dimensional setting can be neglected as the corresponding moments are zero. The size of the angular basis depending on the spatial dimension can be found in Table 1.*

symmetry assumption	spatial dimension	no. spherical harmonics
rotational symmetry around z-axis	1D	$N + 1$
symmetry along z-axis	2D	$\frac{1}{2}N^2 + \frac{3}{2}N + 1$
no symmetry: full problem	3D	$N^2 + 2N + 1$

Table 1: Size of angular basis

3. Second-order formulation of the P_N equations: $\mathbf{P}_N^{2\text{nd}}$

In this section we reformulate the P_N equations described above as system of second-order PDEs in the space variable. This formulation has a simple structure and can easily be handed to a standard PDE tool, like demonstrated in our implementation [22].

Remark 3.1 (Smoothness). *We would like to note that the formal derivation requires additional smoothness of the solution, i.e., equivalence of the two formulations is only given for P_N solutions with the sufficient regularity. Furthermore we do not discuss the well-posedness of the resulting second-order system here.*

⁵We use the normalized Legendre polynomials despite the inconsistency with the literature, where typically the unnormalized Legendre polynomials are used in slab geometry.

3.1. Algebraic transformations

The reformulation of the P_N equations in second-order form is based on the parity property w.r.t. Ω of the real spherical harmonics:

$$S_l^m(-\Omega) = (-1)^l S_l^m(\Omega).$$

The real spherical harmonics are called even / odd if the corresponding degree l is even / odd. In the following we only consider odd values for the order N . We organize the basis functions into even and odd functions⁶

$$\begin{aligned} \mathbf{b}_e &:= (S_0^0, S_{-2}^2, \dots, S_2^2, S_{-4}^4, \dots, S_4^4, \dots, S_{-N+1}^{N-1}, \dots, S_{N-1}^{N-1}), \\ \mathbf{b}_o &:= (S_{-1}^1, \dots, S_1^1, S_{-3}^3, \dots, S_3^3, \dots, S_{-N}^N, \dots, S_N^N) \end{aligned}$$

and rearrange the moments $\mathbf{u}_e = \langle \mathbf{b}_e \hat{I} \rangle$ and $\mathbf{u}_o = \langle \mathbf{b}_o \hat{I} \rangle$, respectively. We define $N_e, N_o \in \mathbb{N}$ to be the sizes of \mathbf{u}_e and \mathbf{u}_o , respectively, i.e., $N_e + N_o = N$.

We can then rewrite the P_N ansatz (11) as

$$\hat{I}(\mathbf{x}, \Omega) = \mathbf{b}_e^T(\Omega) \mathbf{u}_e + \mathbf{b}_o^T(\Omega) \mathbf{u}_o. \quad (15)$$

In particular, with $\Omega_x, \Omega_y, \Omega_z$ being odd functions w.r.t. Ω , we can find that the flux matrices in Equation (12) decouple, since

$$\left(\begin{array}{c} \langle (\nabla_{\mathbf{x}} \cdot \Omega) \mathbf{b}_e \hat{I} \rangle \\ \langle (\nabla_{\mathbf{x}} \cdot \Omega) \mathbf{b}_o \hat{I} \rangle \end{array} \right) \stackrel{(15)}{=} \left(\begin{array}{c} \langle (\nabla_{\mathbf{x}} \cdot \Omega) \mathbf{b}_e \mathbf{b}_e^T \rangle \mathbf{u}_e + \langle (\nabla_{\mathbf{x}} \cdot \Omega) \mathbf{b}_e \mathbf{b}_o^T \rangle \mathbf{u}_o \\ \langle (\nabla_{\mathbf{x}} \cdot \Omega) \mathbf{b}_o \mathbf{b}_e^T \rangle \mathbf{u}_e + \langle (\nabla_{\mathbf{x}} \cdot \Omega) \mathbf{b}_o \mathbf{b}_o^T \rangle \mathbf{u}_o \end{array} \right) \stackrel{\text{parity}}{=} \left(\begin{array}{c} \langle (\nabla_{\mathbf{x}} \cdot \Omega) \mathbf{b}_e \mathbf{b}_e^T \rangle \mathbf{u}_o \\ \langle (\nabla_{\mathbf{x}} \cdot \Omega) \mathbf{b}_o \mathbf{b}_e^T \rangle \mathbf{u}_e \end{array} \right).$$

Remark 3.2. *The fact that the P_N equations decouple is a well-known result. E.g., in [4] this was used to derive an efficient implementation for the time-dependent P_N equations, where the decoupled structure was employed on a staggered grid.*

The P_N system can thus be rewritten as

$$\underbrace{T_{eo}(\mathbf{u}_o)}_{T_{eo}(\mathbf{u}_o)} := \underbrace{T_{eo}^x \partial_x \mathbf{u}_o + T_{eo}^y \partial_y \mathbf{u}_o + T_{eo}^z \partial_z \mathbf{u}_o}_{T_{eo}(\mathbf{u}_o)} = \underbrace{(\sigma_s \Sigma_{ee} - \sigma_t E_{N_e})}_{C_{ee} :=} \mathbf{u}_e + \underbrace{\sigma_s \Sigma_{eo}}_{C_{eo} :=} \mathbf{u}_o, \quad (16a)$$

$$\underbrace{T_{oe}(\mathbf{u}_e)}_{T_{oe}(\mathbf{u}_e)} := \underbrace{T_{oe}^x \partial_x \mathbf{u}_e + T_{oe}^y \partial_y \mathbf{u}_e + T_{oe}^z \partial_z \mathbf{u}_e}_{T_{oe}(\mathbf{u}_e)} = \underbrace{\sigma_s \Sigma_{oe}}_{C_{oe} :=} \mathbf{u}_e + \underbrace{(\sigma_s \Sigma_{oo} - \sigma_t E_{N_o})}_{C_{oo} :=} \mathbf{u}_o, \quad (16b)$$

where $T_{eo}^i := \langle \Omega_i \mathbf{b}_e \mathbf{b}_o^T \rangle$ and $T_{oe}^i := \langle \Omega_i \mathbf{b}_o \mathbf{b}_e^T \rangle$ for $i \in \{x, y, z\}$ and $\Sigma_{ee}, \dots, \Sigma_{oo}$ are the rows and columns of Σ according to the reordering of $\mathbf{u} = (\mathbf{u}_e, \mathbf{u}_o)^T$. Here, T_e and T_o define formal linear differential operators. In Lemma 3.6 we will show, that $C_{oo} \in \mathbb{R}^{N_o \times N_o}$ is invertible (under the assumption of $\sigma_t > 0$). We can then formally solve Equation (16b) for \mathbf{u}_o , i.e.,

$$\mathbf{u}_o = C_{oo}^{-1} (T_o(\mathbf{u}_e) - C_{oe} \mathbf{u}_e), \quad (17)$$

and plug it into Equation (16a) to obtain a second-order system of linear, stationary drift-diffusion equations:

$$T_e (C_{oo}^{-1} (T_o(\mathbf{u}_e) - C_{oe} \mathbf{u}_e)) = C_{ee} \mathbf{u}_e + C_{eo} C_{oo}^{-1} (T_o(\mathbf{u}_e) - C_{oe} \mathbf{u}_e). \quad (18)$$

Assumption 3.3 (No-drift). *Assume that the kernel κ is chosen in such a way that $C_{oe} = 0$ and $C_{eo} = 0$.*

Based on Assumption 3.3 the second-order formulation reduces to

$$T_e (C_{oo}^{-1} (T_o(\mathbf{u}_e))) = C_{ee} \mathbf{u}_e. \quad (19)$$

Note that C_{oo} depends on the quantities σ_s and σ_a and thus cannot be pulled out of the differential operator if the physical coefficients are not space-homogeneous.

⁶For slab geometry and two-dimensional geometry, the reduction has to be performed accordingly.

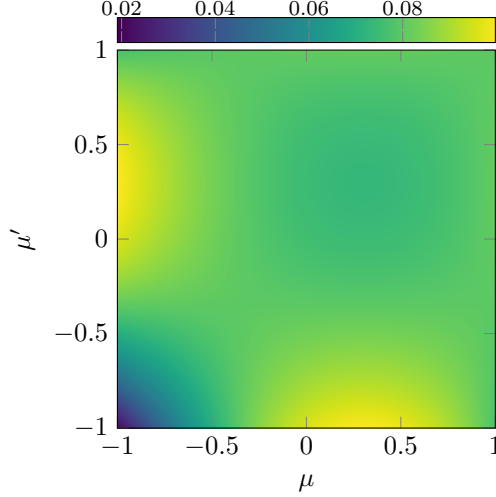


Figure 1: Surface plot of the kernel in Equation (20), which violates the no-drift assumption (Assumption 3.3). The value of $\kappa(\Omega, \Omega')$ is encoded in the color scale.

Remark 3.4. We would like to point out that the previous Assumption 3.3 is necessary to get rid of the drift terms in Equation (18). Even though many kernels satisfying Assumption 2.1 also satisfy Assumption 3.3, this is not true in general, see, e.g.,

$$\kappa(\Omega, \Omega') = \frac{3(25\mu^2 + 25(\mu')^2 - 75\mu^2(\mu')^2 + 45\mu^2\mu' + 45\mu(\mu')^2 - 27\mu\mu' - 15\mu - 15\mu' + 150)}{1900\pi} \quad (20)$$

which yields for $N = 3$ the matrix

$$\Sigma_{eo} = \begin{pmatrix} 0 & 0 & 0 & 0 & 0 & 0 & 0 & 0 & 0 & 0 \\ 0 & 0 & 0 & 0 & 0 & 0 & 0 & 0 & 0 & 0 \\ 0 & 0 & 0 & 0 & 0 & 0 & 0 & 0 & 0 & 0 \\ 0 & \frac{6\sqrt{15}}{475} & 0 & 0 & 0 & 0 & 0 & 0 & 0 & 0 \\ 0 & 0 & 0 & 0 & 0 & 0 & 0 & 0 & 0 & 0 \\ 0 & 0 & 0 & 0 & 0 & 0 & 0 & 0 & 0 & 0 \end{pmatrix}.$$

A plot of this kernel (projected onto the z -component) is given in Figure 1. However, numerical tests (`checkKernelAssumption.m`) have shown that many physically relevant kernels do satisfy this assumption (without proof), like linearly anisotropic scattering (Eddington scattering), Rayleigh scattering, Kagiwada-Kalaba scattering or the von-Mises-Fischer scattering [60–63]. Especially those kernels satisfying the assumption in Lemma 3.5 have the desired property.

Lemma 3.5 (No drift). *Let the kernel κ satisfy Assumption 2.1 and furthermore $\kappa(\Omega, \Omega') = \hat{\kappa}(\Omega^T \Omega')$ for all $\Omega, \Omega' \in \mathcal{S}^2$. Then the kernel satisfies Assumption 3.3, i.e., no drift terms occur in the resulting P_N^{2nd} formulation. In particular, this holds true for the kernels in Examples 2.2 and 2.3.*

Proof. We only show the result for $\hat{\kappa}(\xi)$ even, i.e., $\hat{\kappa}(\xi) = \hat{\kappa}(-\xi)$. The case of $\hat{\kappa}(\xi)$ odd works analogously. The final result then follows by considering the even-odd decomposition of the general kernel as $\hat{\kappa}(\xi) = \hat{\kappa}_e(\xi) + \hat{\kappa}_o(\xi)$, where $\hat{\kappa}_e(\xi) = \frac{1}{2}(\hat{\kappa}(\xi) + \hat{\kappa}(-\xi))$ and $\hat{\kappa}_o(\xi) = \frac{1}{2}(\hat{\kappa}(\xi) - \hat{\kappa}(-\xi))$ denote the even and odd parts of $\hat{\kappa}(\xi)$, respectively.

Let $\mathcal{R} \in \mathbb{R}^{3 \times 3}$ be any rotation matrix that rotates Ω to e_3 , i.e., $\mathcal{R}\Omega = e_3$ with $\det(\mathcal{R}) = 1$. We define the new parametrization of Ω' as $\hat{\Omega} = \left(\sqrt{1 - \hat{\mu}^2} \cos(\hat{\varphi}), \sqrt{1 - \hat{\mu}^2} \sin(\hat{\varphi}), \hat{\mu} \right)^T := \mathcal{R}\Omega'$. Due to the choice of our

angular basis it can be shown [8, 32] that there is a rotation matrix $R(\boldsymbol{\Omega}) \in \mathbb{R}^{N_o \times N_o}$ with

$$\mathbf{b}_o(\mathcal{R}^T \hat{\boldsymbol{\Omega}}) = R^T(\boldsymbol{\Omega}) \mathbf{b}_o(\hat{\boldsymbol{\Omega}}),$$

respectively for the vector of even basis functions. Then we have by the substitution rule that

$$\begin{aligned} \Sigma_{eo} &= \int_{\mathcal{S}^2} \int_{\mathcal{S}^2} \mathbf{b}_e(\boldsymbol{\Omega}) \mathbf{b}_o^T(\boldsymbol{\Omega}') \hat{\kappa}(\boldsymbol{\Omega}^T \boldsymbol{\Omega}') \, d\boldsymbol{\Omega}' \, d\boldsymbol{\Omega} = \int_{\mathcal{S}^2} \int_{-1}^1 \int_0^{2\pi} \mathbf{b}_e(\boldsymbol{\Omega}) \mathbf{b}_o^T(\mathcal{R}^T \hat{\boldsymbol{\Omega}}) \hat{\kappa}(\hat{\boldsymbol{\mu}}) \, d\hat{\varphi} \, d\hat{\mu} \, d\boldsymbol{\Omega} \\ &= \int_{\mathcal{S}^2} \mathbf{b}_e(\boldsymbol{\Omega}) \int_{-1}^1 \int_0^{2\pi} \mathbf{b}_o^T(\mathcal{R}^T \hat{\boldsymbol{\Omega}}) \hat{\kappa}(\hat{\boldsymbol{\mu}}) \, d\hat{\varphi} \, d\hat{\mu} \, d\boldsymbol{\Omega} = \int_{\mathcal{S}^2} \mathbf{b}_e(\boldsymbol{\Omega}) \int_{-1}^1 \int_0^{2\pi} \mathbf{b}_o^T(\hat{\boldsymbol{\Omega}}) \hat{\kappa}(\hat{\boldsymbol{\mu}}) \, d\hat{\varphi} \, d\hat{\mu} R(\boldsymbol{\Omega}) \, d\boldsymbol{\Omega}. \end{aligned}$$

We now only consider the inner integral:

$$\begin{aligned} \int_{-1}^1 \int_0^{2\pi} \mathbf{b}_o^T(\hat{\boldsymbol{\Omega}}) \hat{\kappa}(\hat{\boldsymbol{\mu}}) \, d\hat{\varphi} \, d\hat{\mu} &= \int_0^1 \int_0^{2\pi} \mathbf{b}_o^T(\hat{\boldsymbol{\Omega}}) \hat{\kappa}(\hat{\boldsymbol{\mu}}) \, d\hat{\varphi} \, d\hat{\mu} + \int_{-1}^0 \int_0^{2\pi} \mathbf{b}_o^T(\hat{\boldsymbol{\Omega}}) \hat{\kappa}(\hat{\boldsymbol{\mu}}) \, d\hat{\varphi} \, d\hat{\mu} \\ &= \int_0^1 \int_0^{2\pi} \mathbf{b}_o^T(\hat{\boldsymbol{\Omega}}) \hat{\kappa}(\hat{\boldsymbol{\mu}}) \, d\hat{\varphi} \, d\hat{\mu} + \int_0^1 \int_0^{2\pi} \mathbf{b}_o^T \left(\begin{pmatrix} \sqrt{1-\hat{\mu}^2} \cos(\hat{\varphi}) \\ \sqrt{1-\hat{\mu}^2} \sin(\hat{\varphi}) \\ -\hat{\mu} \end{pmatrix} \right) \hat{\kappa}(-\hat{\boldsymbol{\mu}}) \, d\hat{\varphi} \, d\hat{\mu} \\ &= \int_0^1 \int_0^{2\pi} \mathbf{b}_o^T(\hat{\boldsymbol{\Omega}}) \hat{\kappa}(\hat{\boldsymbol{\mu}}) \, d\hat{\varphi} \, d\hat{\mu} + \int_0^1 \int_{-\pi}^{\pi} \mathbf{b}_o^T \left(\begin{pmatrix} \sqrt{1-\hat{\mu}^2} \cos(\hat{\varphi} + \pi) \\ \sqrt{1-\hat{\mu}^2} \sin(\hat{\varphi} + \pi) \\ -\hat{\mu} \end{pmatrix} \right) \hat{\kappa}(-\hat{\boldsymbol{\mu}}) \, d\hat{\varphi} \, d\hat{\mu} \\ &= \int_0^1 \int_0^{2\pi} \mathbf{b}_o^T(\hat{\boldsymbol{\Omega}}) \hat{\kappa}(\hat{\boldsymbol{\mu}}) \, d\hat{\varphi} \, d\hat{\mu} + \int_0^1 \int_{-\pi}^{\pi} \mathbf{b}_o^T(-\hat{\boldsymbol{\Omega}}) \hat{\kappa}(-\hat{\boldsymbol{\mu}}) \, d\hat{\varphi} \, d\hat{\mu} \\ &\stackrel{\substack{\hat{\kappa}(\xi) \text{ even} \\ \text{parity}}}{=} \int_0^1 \int_0^{2\pi} \mathbf{b}_o^T(\hat{\boldsymbol{\Omega}}) \hat{\kappa}(\hat{\boldsymbol{\mu}}) \, d\hat{\varphi} \, d\hat{\mu} - \int_0^1 \int_{-\pi}^{\pi} \mathbf{b}_o^T(\hat{\boldsymbol{\Omega}}) \hat{\kappa}(\hat{\boldsymbol{\mu}}) \, d\hat{\varphi} \, d\hat{\mu} \\ &= \int_0^1 \int_0^{2\pi} \mathbf{b}_o^T(\hat{\boldsymbol{\Omega}}) \hat{\kappa}(\hat{\boldsymbol{\mu}}) \, d\hat{\varphi} \, d\hat{\mu} - \int_0^1 \int_0^{2\pi} \mathbf{b}_o^T(\hat{\boldsymbol{\Omega}}) \hat{\kappa}(\hat{\boldsymbol{\mu}}) \, d\hat{\varphi} \, d\hat{\mu} = 0, \end{aligned}$$

where we used that the $\sin(\varphi)$ and $\cos(\varphi)$ are periodic in the last equality. Thus, $\Sigma_{eo} = 0$ as well. The proof works in the same way for odd kernels, where we define the rotation matrix such that $\mathcal{R}\boldsymbol{\Omega}' = e_3$, and $\hat{\boldsymbol{\Omega}} = \mathcal{R}\boldsymbol{\Omega}$, and only consider the integral with respect to $\boldsymbol{\Omega}$. \square

We now want to show that the reduction operator (17) is well-defined.

Lemma 3.6 (Solving for \mathbf{u}_o in Equation (16b)). *Let the kernel κ satisfy Assumption 2.1. The matrix $C_{oo} = (\sigma_s \Sigma_{oo} - \sigma_t E_{N_o})$ is invertible whenever $\sigma_a + \sigma_s = \sigma_t > 0$.*

Proof. We have that

$$\Sigma_{oo} = \int_{\mathcal{S}^2} \int_{\mathcal{S}^2} \mathbf{b}_o(\boldsymbol{\Omega}) \mathbf{b}_o(\boldsymbol{\Omega}')^T \kappa(\boldsymbol{\Omega}, \boldsymbol{\Omega}') \, d\boldsymbol{\Omega}' \, d\boldsymbol{\Omega},$$

especially Σ_{oo} is symmetric due to the symmetry of κ . Let $\mathbf{c} \in \mathbb{R}^{N_o}$ and we define $a(\boldsymbol{\Omega}) := \mathbf{c}^T \mathbf{b}_o(\boldsymbol{\Omega})$, then

it holds:

$$\begin{aligned}
\mathbf{c}^T (\sigma_s \Sigma_{\text{oo}} - \sigma_t E_{N_o}) \mathbf{c} &= \sigma_s \int_{\mathcal{S}^2} \int_{\mathcal{S}^2} \kappa(\boldsymbol{\Omega}, \boldsymbol{\Omega}') a(\boldsymbol{\Omega}) a(\boldsymbol{\Omega}') \, \text{d}\boldsymbol{\Omega}' \, \text{d}\boldsymbol{\Omega} - \sigma_t \|\mathbf{c}\|_2^2 \\
&= \frac{\sigma_s}{2} \int_{\mathcal{S}^2} \int_{\mathcal{S}^2} \kappa(\boldsymbol{\Omega}, \boldsymbol{\Omega}') \left(a^2(\boldsymbol{\Omega}) + a^2(\boldsymbol{\Omega}') - (a(\boldsymbol{\Omega}) - a(\boldsymbol{\Omega}'))^2 \right) \, \text{d}\boldsymbol{\Omega}' \, \text{d}\boldsymbol{\Omega} - \sigma_t \|\mathbf{c}\|_2^2 \\
&\stackrel{\text{(A2)}}{=} \sigma_s \langle a^2 \rangle - \frac{\sigma_s}{2} \int_{\mathcal{S}^2} \int_{\mathcal{S}^2} \kappa(\boldsymbol{\Omega}, \boldsymbol{\Omega}') (a(\boldsymbol{\Omega}) - a(\boldsymbol{\Omega}'))^2 \, \text{d}\boldsymbol{\Omega}' \, \text{d}\boldsymbol{\Omega} - \sigma_t \|\mathbf{c}\|_2^2 \\
&\stackrel{\text{(A3)}}{\leq} \sigma_s \langle a^2 \rangle - \frac{\sigma_s}{2} \int_{\mathcal{S}^2} \int_{\mathcal{S}^2} \kappa_0 (a(\boldsymbol{\Omega}) - a(\boldsymbol{\Omega}'))^2 \, \text{d}\boldsymbol{\Omega}' \, \text{d}\boldsymbol{\Omega} - \sigma_t \|\mathbf{c}\|_2^2 \\
&\stackrel{\text{(A1)}}{\leq} \sigma_s \langle a^2 \rangle - \frac{\sigma_s}{2} \int_{\mathcal{S}^2} \int_{\mathcal{S}^2} \kappa_0 (a(\boldsymbol{\Omega}) - a(\boldsymbol{\Omega}'))^2 \, \text{d}\boldsymbol{\Omega}' \, \text{d}\boldsymbol{\Omega} - \sigma_t \|\mathbf{c}\|_2^2 \\
&= \sigma_s (1 - \kappa_0) \langle a^2 \rangle + \sigma_s \kappa_0 \int_{\mathcal{S}^2} \int_{\mathcal{S}^2} a(\boldsymbol{\Omega}) a(\boldsymbol{\Omega}') \, \text{d}\boldsymbol{\Omega}' \, \text{d}\boldsymbol{\Omega} - \sigma_t \|\mathbf{c}\|_2^2 \\
&\stackrel{\text{(21)}}{=} \sigma_s (1 - \kappa_0) \langle a^2 \rangle - \sigma_t \|\mathbf{c}\|_2^2 \stackrel{\text{(22)}}{=} (\sigma_s (1 - \kappa_0) - \sigma_t) \|\mathbf{c}\|_2^2 = -(\sigma_s \kappa_0 + \sigma_a) \|\mathbf{c}\|_2^2,
\end{aligned}$$

where we used that

$$\int_{\mathcal{S}^2} a(\boldsymbol{\Omega}) \, \text{d}\boldsymbol{\Omega} = \mathbf{c}^T \int_{\mathcal{S}^2} \mathbf{b}_o(\boldsymbol{\Omega}) \, \text{d}\boldsymbol{\Omega} = 0, \tag{21}$$

as every entry in \mathbf{b}_o is orthogonal to $b_0 = \frac{1}{\sqrt{4\pi}}$ and thus to all constants w.r.t. $\langle \cdot \rangle$, and

$$\langle a^2 \rangle = \mathbf{c}^T \int_{\mathcal{S}^2} \mathbf{b}_o \mathbf{b}_o^T \, \text{d}\boldsymbol{\Omega} \mathbf{c} \stackrel{\text{ONB}}{=} \mathbf{c}^T \mathbf{c} = \|\mathbf{c}\|_2^2. \tag{22}$$

In particular, since $\sigma_t = \sigma_a + \sigma_s > 0$ and $\kappa_0 > 0$, we get that $\sigma_s \kappa_0 + \sigma_a > 0$, which implies that C_{oo} is negative definite and therefore invertible. \square

3.2. Weak formulation and boundary conditions

One major problem of the P_N equations is that the boundary conditions (4) of the transfer equation have to be prescribed for inward-pointing angles ($\mathbf{n} \cdot \boldsymbol{\Omega} < 0$) only, whereas the hyperbolic P_N system requires information for the characteristic variables related to ingoing characteristics [64]. Although these quantities are somehow related, a consistent approximation of boundary conditions for moment models is non-trivial [65–69].

Without thinking too much about these implications for the P_N equations, we want to use the Marshak approach to derive consistent boundary conditions for Equation (18). The basic idea is to replace I in Equation (4) with the P_N ansatz \hat{I} and take half moments over $\mathbf{n} \cdot \boldsymbol{\Omega} < 0$ of the equation w.r.t. to a suitable subset of basis functions. Using all basis functions would provide more boundary conditions than actually needed. The choice of “all relevant” basis functions is also discussed in [9]. We choose all odd basis functions in \mathbf{b}_o for the half moments at the boundary as those are the ones which appear naturally in the weak formulation as discussed below. This also leads to more equations than unknowns but guarantees the existence of the second-order formulation as shown in Lemma 3.7. Whereas we reason with the existence of our second-order formulation for this particular choice of basis functions, this choice was already taken before in literature, e.g., in a classical SP_N context in [70].

We start to derive the weak form for \mathbf{u}_e . Let v denote a suitable spatial test function and $i \in \{1, \dots, N_e\}$.

The weak form then reads

$$\begin{aligned}
& \int_X (C_{ee})_i \mathbf{u}_e v \, d\mathbf{x} \\
& \stackrel{(16a)}{=} \int_X (T_e(\mathbf{u}_o))_i v \, d\mathbf{x} = \int_X (\langle \boldsymbol{\Omega}_x (\mathbf{b}_e)_i \mathbf{b}_o^T \rangle \partial_x \mathbf{u} + \langle \boldsymbol{\Omega}_y (\mathbf{b}_e)_i \mathbf{b}_o^T \rangle \partial_y \mathbf{u} + \langle \boldsymbol{\Omega}_z (\mathbf{b}_e)_i \mathbf{b}_o^T \rangle \partial_z \mathbf{u}) v \, d\mathbf{x} \quad (23) \\
& = \int_X \nabla \cdot \langle \boldsymbol{\Omega} (\mathbf{b}_e)_i \mathbf{b}_o^T \mathbf{u}_o \rangle v \, d\mathbf{x} \stackrel{\text{Gauss}}{=} - \int_X \langle \boldsymbol{\Omega} (\mathbf{b}_e)_i \mathbf{b}_o^T \mathbf{u}_o \rangle \nabla v \, d\mathbf{x} + \int_\Gamma \langle (\mathbf{n} \cdot \boldsymbol{\Omega}) (\mathbf{b}_e)_i \mathbf{b}_o^T \mathbf{u}_o \rangle v \, ds,
\end{aligned}$$

where we used the divergence theorem in the last step. We now want to eliminate \mathbf{u}_o in Equation (23) using the boundary conditions. Therefore we consider half moments of Equation (4) with respect to the odd basis functions:

$$\int_{\mathbf{n} \cdot \boldsymbol{\Omega} < 0} \mathbf{b}_o (I(\mathbf{x}, \boldsymbol{\Omega}) - \rho I(\mathbf{x}, r(\boldsymbol{\Omega}))) \, d\boldsymbol{\Omega} = \underbrace{\int_{\mathbf{n} \cdot \boldsymbol{\Omega} < 0} (1 - \rho) \mathbf{b}_o I_\Gamma(\mathbf{x}, \boldsymbol{\Omega}) \, d\boldsymbol{\Omega}}_{\mathbf{u}_\Gamma}. \quad (24)$$

We note that \mathbf{u}_Γ might depend on the position \mathbf{x} as well as the orientation of the boundary, i.e., the unit outer normal vector \mathbf{n} . Plugging in the definition of the ansatz (15) yields

$$\left(\int_{\mathbf{n} \cdot \boldsymbol{\Omega} < 0} \mathbf{b}_o(\boldsymbol{\Omega}) (\mathbf{b}_o^T(\boldsymbol{\Omega}) - \rho \mathbf{b}_o^T(r(\boldsymbol{\Omega}))) \, d\boldsymbol{\Omega} \right) \cdot \mathbf{u}_o + \left(\int_{\mathbf{n} \cdot \boldsymbol{\Omega} < 0} \mathbf{b}_o(\boldsymbol{\Omega}) (\mathbf{b}_e^T(\boldsymbol{\Omega}) - \rho \mathbf{b}_e^T(r(\boldsymbol{\Omega}))) \, d\boldsymbol{\Omega} \right) \cdot \mathbf{u}_e = \mathbf{u}_\Gamma.$$

Defining the matrices

$$H_o(\mathbf{n}) := \int_{\mathbf{n} \cdot \boldsymbol{\Omega} < 0} \mathbf{b}_o(\boldsymbol{\Omega}) (\mathbf{b}_o^T(\boldsymbol{\Omega}) - \rho \mathbf{b}_o^T(r(\boldsymbol{\Omega}))) \, d\boldsymbol{\Omega}, \quad (25a)$$

$$H_e(\mathbf{n}) := \int_{\mathbf{n} \cdot \boldsymbol{\Omega} < 0} \mathbf{b}_o(\boldsymbol{\Omega}) (\mathbf{b}_e^T(\boldsymbol{\Omega}) - \rho \mathbf{b}_e^T(r(\boldsymbol{\Omega}))) \, d\boldsymbol{\Omega} \quad (25b)$$

we are able to rewrite the equation above, given that the matrix $H_o(\mathbf{n})$ is invertible (see Lemma 3.7), as

$$\mathbf{u}_o = \mathbf{u}_o(\mathbf{x}) = H_o(\mathbf{n})^{-1} (\mathbf{u}_\Gamma - H_e(\mathbf{n}) \mathbf{u}_e) \quad (\text{for } \mathbf{x} \in \Gamma). \quad (26)$$

Thus, the final weak form reads

$$\begin{aligned}
& \int_X \langle \boldsymbol{\Omega} (\mathbf{b}_e)_i \mathbf{b}_o^T C_{oo}^{-1} T_o(\mathbf{u}_e) \rangle \cdot \nabla v \, d\mathbf{x} + \int_X (C_{ee})_i \mathbf{u}_e v \, d\mathbf{x} + \int_\Gamma \langle (\mathbf{n} \cdot \boldsymbol{\Omega}) (\mathbf{b}_e)_i \mathbf{b}_o^T \rangle H_o(\mathbf{n})^{-1} H_e(\mathbf{n}) \mathbf{u}_e v \, ds \quad (27) \\
& = \int_\Gamma \langle (\mathbf{n} \cdot \boldsymbol{\Omega}) (\mathbf{b}_e)_i \mathbf{b}_o^T \rangle H_o(\mathbf{n})^{-1} \mathbf{u}_\Gamma v \, ds.
\end{aligned}$$

It remains to show, that the reduction (26) is well-defined.

Lemma 3.7 (Solving for \mathbf{u}_o in Equation (26)). *The matrix $H_o(\mathbf{n})$ is invertible for all $\rho \in (-1, 1)$.*

Proof. The rotation matrix that rotates a vector around the axis $\mathbf{n} = [n_x \ n_y \ n_z]$ by an angle of 180° is given by

$$\mathcal{R} = \begin{pmatrix} 2n_x^2 - 1 & 2n_x n_y & 2n_x n_z \\ 2n_y n_x & 2n_y^2 - 1 & 2n_y n_z \\ 2n_z n_x & 2n_z n_y & 2n_z^2 - 1 \end{pmatrix}.$$

The reflection of $\boldsymbol{\Omega}$ at the plane $\{\boldsymbol{\Omega} \in \mathcal{S}^2 : \mathbf{n} \cdot \boldsymbol{\Omega} = 0\}$ can be represented by a rotation around \mathbf{n} by an angle of 180° and a subsequent negation:

$$r(\boldsymbol{\Omega}) = \boldsymbol{\Omega} - 2(\mathbf{n} \cdot \boldsymbol{\Omega})\mathbf{n} = \begin{pmatrix} \Omega_x - 2n_x(\Omega_x n_x + \Omega_y n_y + \Omega_z n_z) \\ \Omega_y - 2n_y(\Omega_x n_x + \Omega_y n_y + \Omega_z n_z) \\ \Omega_z - 2n_z(\Omega_x n_x + \Omega_y n_y + \Omega_z n_z) \end{pmatrix} = -\mathcal{R}\boldsymbol{\Omega}.$$

Like in the proof of Lemma 3.5 there is a rotation matrix $R_\pi(\mathbf{n}) \in \mathbb{R}^{N_o \times N_o}$, only depending on \mathbf{n} , with

$$\mathbf{b}_o(\mathcal{R}\boldsymbol{\Omega}) = R_\pi(\mathbf{n}) \mathbf{b}_o(\boldsymbol{\Omega}).$$

Using the parity of the odd real spherical harmonics, i.e., $\mathbf{b}_o(-\mathcal{R}\boldsymbol{\Omega}) = -\mathbf{b}_o(\mathcal{R}\boldsymbol{\Omega})$, and our assumption, that the reflectivity ρ does not depend on $\boldsymbol{\Omega}$, we can rewrite the matrix as

$$H_o(\mathbf{n}) = \int_{\mathbf{n} \cdot \boldsymbol{\Omega} < 0} \mathbf{b}_o(\boldsymbol{\Omega}) (\mathbf{b}_o^T(\boldsymbol{\Omega}) + \rho \mathbf{b}_o^T(\boldsymbol{\Omega}) R_\pi^T(\mathbf{n})) \, d\boldsymbol{\Omega} = \int_{\mathbf{n} \cdot \boldsymbol{\Omega} < 0} \mathbf{b}_o(\boldsymbol{\Omega}) \mathbf{b}_o^T(\boldsymbol{\Omega}) \, d\boldsymbol{\Omega} (E_{N_o} + \rho R_\pi^T(\mathbf{n})).$$

$H_o(\mathbf{n})$ is thus invertible if $\int_{\mathbf{n} \cdot \boldsymbol{\Omega} < 0} \mathbf{b}_o(\boldsymbol{\Omega}) \mathbf{b}_o^T(\boldsymbol{\Omega}) \, d\boldsymbol{\Omega}$ and $E_{N_o} + \rho R_\pi^T(\mathbf{n})$ are invertible. Consider the vector $\mathbf{c} \in \mathbb{R}^{N_o} \setminus \{0\}$. Then we have that

$$\mathbf{c}^T \int_{\mathbf{n} \cdot \boldsymbol{\Omega} < 0} \mathbf{b}_o(\boldsymbol{\Omega}) \mathbf{b}_o^T(\boldsymbol{\Omega}) \, d\boldsymbol{\Omega} \mathbf{c} = \int_{\mathbf{n} \cdot \boldsymbol{\Omega} < 0} (\mathbf{c}^T \mathbf{b}_o(\boldsymbol{\Omega}))^2 \, d\boldsymbol{\Omega} > 0$$

since $\mathbf{c} \neq 0$ and the real spherical harmonics being linearly independent and continuous. Thus, the first matrix in the product is symmetric, positive definite and thus invertible. Using a Neumann series, $E_{N_o} + \rho R_\pi^T(\mathbf{n})$ is invertible if $\|\rho R_\pi^T(\mathbf{n})\| < 1$ for any matrix norm. In particular, since $R_\pi^T(\mathbf{n})$ is a rotation matrix, it has $\|R_\pi^T(\mathbf{n})\|_2 = 1$ (induced operator norm), such that we get $\|\rho R_\pi^T(\mathbf{n})\| < 1$ if $|\rho| < 1$.

We would like to note that using rotation matrices to derive boundary conditions has also been used in a different way in [8, 9]. \square

Remark 3.8. Lemma 3.7 proves the invertibility of the matrix $H_o(\mathbf{n})$ for $\rho \in (-1, 1)$, which especially includes our case $\rho \in [0, 1)$.

Remark 3.9. Due to parity and the fact that $r(-\boldsymbol{\Omega}) = -r(\boldsymbol{\Omega})$, we get that $H_o(\mathbf{n}) = H_o(-\mathbf{n})$ and $H_e(\mathbf{n}) = -H_e(-\mathbf{n})$.

Remark 3.10. Using the definitions in Equations (13), (14), (16a), (16b), (25a), (24), (25a) and (25b), we can reformulate the weak form more explicitly as

$$\begin{aligned} & \int_X (K_{xx} \cdot \partial_x \mathbf{u}_e + K_{xy} \cdot \partial_y \mathbf{u}_e + K_{xz} \cdot \partial_z \mathbf{u}_e) \cdot \partial_x \mathbf{v} \, dx + \int_X (K_{yx} \cdot \partial_x \mathbf{u}_e + K_{yy} \cdot \partial_y \mathbf{u}_e + K_{yz} \cdot \partial_z \mathbf{u}_e) \cdot \partial_y \mathbf{v} \, dx \\ & + \int_X (K_{zx} \cdot \partial_x \mathbf{u}_e + K_{zy} \cdot \partial_y \mathbf{u}_e + K_{zz} \cdot \partial_z \mathbf{u}_e) \cdot \partial_z \mathbf{v} \, dx + \int_X C_{ee} \cdot \mathbf{u}_e \cdot \mathbf{v} \, dx + \int_\Gamma B_l \cdot \mathbf{u}_e \cdot \mathbf{v} \, ds \\ & = \int_\Gamma B_r \cdot \mathbf{u}_\Gamma \cdot \mathbf{v} \, ds \end{aligned}$$

with

$$\begin{aligned} K_{xx} &= T_{eo}^x \cdot C_{oo}^{-1} \cdot T_{oe}^x, & K_{xy} &= T_{eo}^x \cdot C_{oo}^{-1} \cdot T_{oe}^y, & K_{xz} &= T_{eo}^x \cdot C_{oo}^{-1} \cdot T_{oe}^z, \\ K_{yx} &= T_{eo}^y \cdot C_{oo}^{-1} \cdot T_{oe}^x, & K_{yy} &= T_{eo}^y \cdot C_{oo}^{-1} \cdot T_{oe}^y, & K_{yz} &= T_{eo}^y \cdot C_{oo}^{-1} \cdot T_{oe}^z, \\ K_{zx} &= T_{eo}^z \cdot C_{oo}^{-1} \cdot T_{oe}^x, & K_{zy} &= T_{eo}^z \cdot C_{oo}^{-1} \cdot T_{oe}^y, & K_{zz} &= T_{eo}^z \cdot C_{oo}^{-1} \cdot T_{oe}^z \end{aligned}$$

Software	Version
MATLAB [17]	9.5.0.944444 (R2018b)
MATLAB's Symbolic Math Toolbox	Version 8.2 (R2018b)
PYTHON [75]	3.6.7
NumPy [76]	1.14.6
SciPy [77]	1.1.0
FEniCS [18]	2018.1.0
Gmsh [78]	3.0.6

Table 2: Used software / versions

and

$$B_l(\mathbf{n}) = \langle (\mathbf{n} \cdot \boldsymbol{\Omega}) \mathbf{b}_e \mathbf{b}_o^T \rangle H_o(\mathbf{n})^{-1} H_e(\mathbf{n}),$$

$$B_r(\mathbf{n}) = \langle (\mathbf{n} \cdot \boldsymbol{\Omega}) \mathbf{b}_e \mathbf{b}_o^T \rangle H_o(\mathbf{n})^{-1}.$$

As demonstrated in the next section a system of this structure can be handed to standard PDE tools like, e.g., FEniCS [18, 19].

4. Numerical Results

The different test cases demonstrate the broad applicability of our approach to different scenarios including heterogeneous coefficients, anisotropic scattering, anisotropic boundary sources and different spatial dimensions. We reduced the computational complexity by looking at reduced problems in one and two space dimensions like described in Section 2.2, whereas we provide code for the full 3D scenario as well.

4.1. Code interface / Implementation details

Our MATLAB code for the evaluation of the real spherical harmonics is based on [32]. We would like to note here that our implementation does not include the Condon-Shortley phase (“ $(-1)^m$ prefactor”) in contrary to, e.g., MATLAB’s legendre function. The (permuted version of the) P_N flux matrices are given explicitly in [4]. We approximate the integrals over (subdomains of) the unit sphere \mathcal{S}^2 by a quadrature rule. This is based on a trigonometric Gaussian quadrature rule for polynomials on a circle, described, e.g., in [71]. We employ the authors implementation of this quadrature rule in MATLAB, provided in [72]. For a detailed investigation in the reduced 2D case, see [30].

In cases for which we do not know the reference solution of the kinetic problem or the original P_N equations, we compare our result to the approximate solution of the discrete ordinates method. For a recent survey and relevant references, see [73]. For our implementation of the discrete ordinates method in 2D we needed barycentric interpolation on the sphere like described in [74].

We discretize the weak formulation of the $P_N^{2\text{nd}}$ systems using linear Lagrange finite elements with the help of FEniCS.

4.2. Test case 1

The first test case is rather simple and we are able to compute analytic reference solutions for the kinetic problem and the original P_N equations, which allows us to validate our code in this setup, which is given in Table 3. It is easy to check that the analytic reference solution for the kinetic problem is given by

$$I_\Gamma(z = 0, \mu \geq 0) = \frac{1}{4\pi} \quad \rho(z = 0) = 0 \quad \sigma_a(z) = 1 \quad X = [0, 1]$$

$$I_\Gamma(z = 1, \mu < 0) = 0 \quad \rho(z = 1) = 0 \quad \sigma_s(z) = 0 \quad \kappa(\boldsymbol{\Omega}, \boldsymbol{\Omega}') = \frac{1}{4\pi}$$

Table 3: Setup for test case 1

$$I(\mathbf{x}, \boldsymbol{\Omega}) = I(z, \mu) = \begin{cases} \frac{1}{4\pi} e^{-\frac{\sigma_a}{\mu} z} & , \mu > 0 \\ 0 & , \mu \leq 0 \end{cases}, \quad (28)$$

$$\phi_{\text{kin}}(z) = 2\pi \int_{-1}^1 I(z, \mu) d\mu. \quad (29)$$

In this simple case we can reformulate the P_N system as an initial value problem. This gives us up to the precision of the solution of the corresponding ODE a reference solution, denoted by ϕ_{P_N} , for the solutions of the P_N^{2nd} approach.

In Figure 2 we present the results of a numerical study of this test case, where we compare different approximations of the radiative energy with the analytic reference solution, see Subfigure 2a. For the discrete ordinates method we use a quadrature rule on the unit sphere which is exact for polynomials up to degree 23 and obtain 50 discrete ordinates after reduction to 1D (by fixing φ and only discretizing μ). Furthermore we look at the convergence of the radiative energies of the P_N solutions to the one of the kinetic reference solution for increasing moment order N , see Subfigure 2b, and the convergence of the radiative energies of the numerical approximations of the P_N^{2nd} equations to the ones of the P_N reference solutions, see Subfigure 2c.

From the analytic solution of the kinetic problem (28) we see that we would need infinitely many real spherical harmonics in the basis expansion to describe the true solution, which gives reason for the slow convergence.

This test case indicates the convergence of the solutions of the P_N method to the true solution of the kinetic problem and furthermore the equivalence of the solutions of the original P_N equations and our second-order formulation (in cases where the derivation is justified).

Referring to our repository on GitHub [22], we list the functions used to compute the different approximations of the distribution and radiative energy in Table 4.

wrapper		<code>runTestCase1.m</code>
kinetic reference solution	ϕ_{kin}	<code>radiativeEnergyKineticSolutionTestCase1.m</code>
discrete ordinates method	ϕ_{DOM}	<code>mainDiscreteOrdinates1D.m</code>
P_N reference solution	ϕ_{P_N}	<code>radiativeEnergyPNOrgIsotropicKernel1D.m</code>
P_N^{2nd} solution	$\phi_{P_N^{\text{2nd}}}$	<code>runTestCase1.py</code>
transformation $P_N \rightarrow P_N^{\text{2nd}}$		<code>generateTestCase1.m</code>

Table 4: Implementation of test case 1

4.3. Test case 2

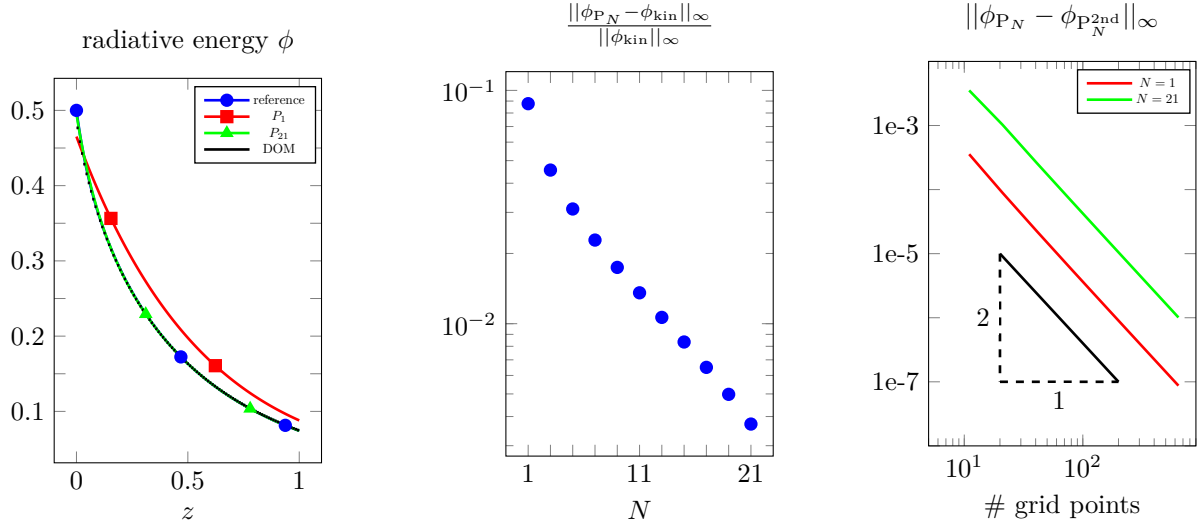
The second test case demonstrates that we are able to treat heterogeneous coefficients, non-vanishing reflectivity at the boundary and anisotropic boundary sources in 1D. The setup for this test case in 1D is given in Table 5. For this test case we are again able to compute a reference solution of the original P_N

$$\begin{aligned} I_{\Gamma}(z=0, \mu \geq 0) &= \mu^2 & \rho(z=0) &= \frac{1}{2} & \sigma_a(z) &= \frac{2+\sin(2\pi z)}{10} & X &= [0, 1] \\ I_{\Gamma}(z=1, \mu < 0) &= 0 & \rho(z=1) &= \frac{1}{2} & \sigma_s(z) &= \frac{3-z^2}{10} & \kappa(\boldsymbol{\Omega}, \boldsymbol{\Omega}') &= \frac{1}{4\pi} \end{aligned}$$

Table 5: Setup for test case 2

system by reformulating this as initial value problem.

In Figure 3 we present the results of a numerical study of this test case, where we compare different approximations of the radiative energy with the approximation by the discrete ordinates method as reference solution, see Subfigure 3a. For the discrete ordinates method we used a quadrature rule on the unit sphere which is exact for polynomials up to degree 23 and obtain 50 ordinates after reduction to 1D (by fixing φ and only discretizing μ). Furthermore we look at the convergence of the radiative energies of the P_N^{2nd} solutions to the one of the discrete ordinates method for increasing moment order N , see Subfigure 3b, and



(a) Radiative energies ϕ of the discrete ordinates solution, the analytic solution of the kinetic problem (reference) and the original P_1 and P_{21} solutions.

(b) Relative maximum distances of the radiative energies of the original P_N solutions to the kinetic problem.

(c) Maximum distances of the original P_N solutions to the numerical solutions of the P_N^{2nd} equations.

Figure 2: Test case 1

the convergence of the radiative energies of the numerical approximations of the P_N^{2nd} equations to the ones of the P_N reference solutions, see Subfigure 3c.

We observe a significant jump already between the first two moment orders.

Referring to our repository on GitHub [22], we list the functions used to compute the different approximations of the distribution and radiative energy in Table 6.

wrapper		<code>runTestCase2.m</code>
discrete ordinates method	ϕ_{DOM}	<code>mainDiscreteOrdinates1D.m</code>
P_N reference solution	ϕ_{P_N}	<code>radiativeEnergyPNOrigIsotropicKernel1D.m</code>
P_N^{2nd} solution	$\phi_{P_N^{2nd}}$	<code>runTestCase2.py</code>
transformation $P_N \rightarrow P_N^{2nd}$		<code>generateTestCase2.m</code>

Table 6: Implementation of test case 2

4.4. Test case 3

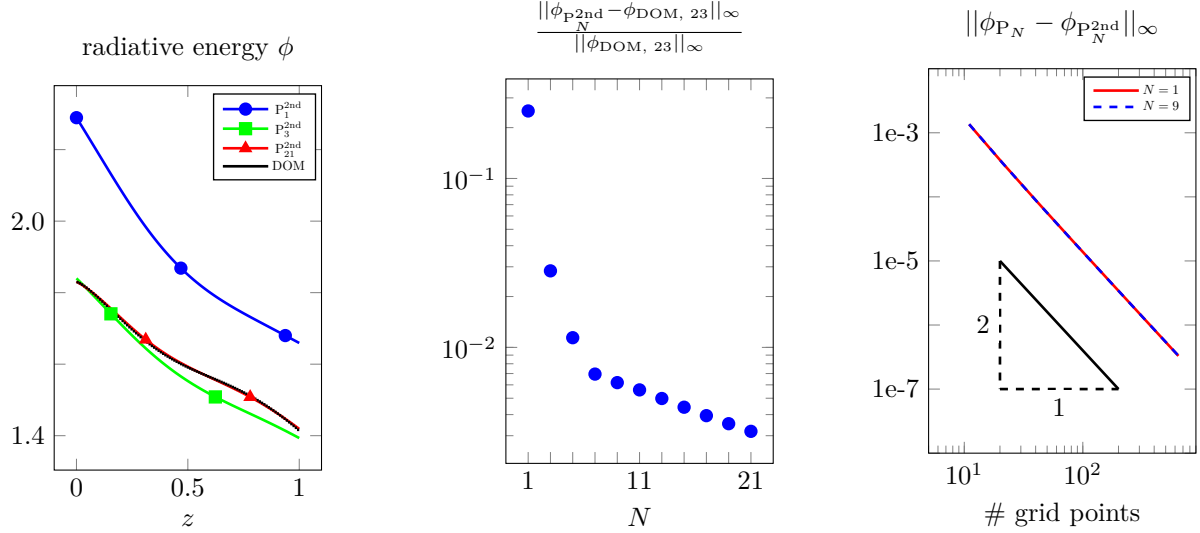
The third test case demonstrates that our method is not limited to isotropic scattering. The setup for this test case in 1D is given in Table 7. We are able to compute an analytic reference solution for the kinetic

$$\begin{aligned}
 I_\Gamma(z=0, \mu \geq 0) &= \mu + 2 & \rho(z=0) &= 0 & \sigma_a(z) &= 0 & X &= [0, 1] \\
 I_\Gamma(z=1, \mu < 0) &= \mu + 1 & \rho(z=1) &= 0 & \sigma_s(z) &= 1 + z & \kappa(\mathbf{\Omega}, \mathbf{\Omega}') &= \frac{1}{8\pi}((\mu - 1)(\mu' - 1) + (\mu + 1)(\mu' + 1))
 \end{aligned}$$

Table 7: Setup for test case 3

problem, which reads:

$$I(\mathbf{x}, \mathbf{\Omega}) = \mu - \frac{z(z+2)}{3} + 2. \quad (30)$$



(a) Radiative energies ϕ of the discrete ordinates solution and the numerical solutions of the P_1^{2nd} , P_3^{2nd} and P_{21}^{2nd} equations.

(b) Relative maximum distances of the radiative energies of the discrete ordinates solution to the numerical solutions of P_N^{2nd} equations.

(c) Maximum distances of the solutions of the original P_N equations to the numerical solutions of P_N^{2nd} equations.

Figure 3: Test case 2

We see that the analytic solution is a first-order polynomial in Ω , thus we expect that the solution of the P_1 equations should give the exact solution of the kinetic problem.

In Figure 4 we present the results of a numerical study of this test case, where we compare different approximations of the radiative energy with the analytic reference solution, see Subfigure 4a. For the discrete ordinates method we use a quadrature rule on the unit sphere which is exact for polynomials up to degree 23, where we did not reduce the set of ordinates in this case and ended up with 600 discrete ordinates on the full sphere. Furthermore we look at the convergence of the radiative energies of the numerical approximations of the P_N^{2nd} by comparing the solution on a certain grid to the one on a refined grid, see Subfigure 4b.

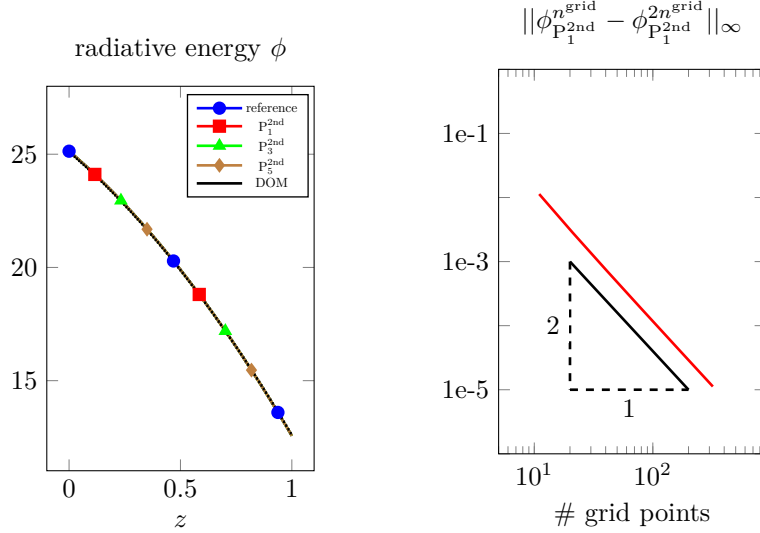
Referring to our repository on GitHub [22], we list the functions used to compute the different approximations of the distribution and radiative energy in Table 8.

wrapper		<code>runTestCase3.m</code>
kinetic reference solution	ϕ_{kin}	<code>radiativeEnergyKineticSolutionTestCase3.m</code>
discrete ordinates method	ϕ_{DOM}	<code>mainDiscreteOrdinates1D.m</code>
P_N^{2nd} solution	$\phi_{P_N^{2nd}}$	<code>runTestCase3.py</code>
transformation $P_N \rightarrow P_N^{2nd}$		<code>generateTestCase3.m</code>

Table 8: Implementation of test case 3

4.5. Test case 4

This test case demonstrates that our method can deal with heterogeneous coefficients in 2D. It is based on the shadow test [39, 50] which represents a particle stream that is partially blocked by an absorber, resulting in a shadowed region behind the absorber. The setup for this test case in 2D is given in Table 9, based on the auxiliary functions in Equation (31). The domain X and the partition of the boundary $\Gamma = \Gamma_I \cup \Gamma_{II} \cup \Gamma_{III} \cup \Gamma_{IV}$ are illustrated in Figure 6a.



(a) Radiative energies ϕ of the discrete ordinates solution, the analytic solution of the kinetic problem (reference) and the numerical solutions of the P_1^{2nd} , P_3^{2nd} and P_5^{2nd} equations. (b) Maximum distances of the numerical solutions of the P_1^{2nd} equations on equidistant grids with n^{grid} and $2n^{\text{grid}}$ nodes.

Figure 4: Test case 3

$$f_1(\mathbf{x}) = \begin{cases} \exp(-100(x-0.6)^2) & , x \leq 0.6 \\ 1 & , x > 0.6 \end{cases}, \quad (31a)$$

$$f_2(\mathbf{x}) = \begin{cases} \exp(-100(x-0.7)^2) & , x \geq 0.7 \\ 1 & , x < 0.7 \end{cases}, \quad (31b)$$

$$f_3(\mathbf{x}) = \begin{cases} \exp(-100(y-0.4)^2) & , y \geq 0.4 \\ 1 & , y < 0.4 \end{cases}. \quad (31c)$$

$$\begin{aligned} X &= [0, 3] \times [0, 1] & \kappa(\mathbf{\Omega}, \mathbf{\Omega}') &= \frac{1}{4\pi} & \sigma_a &= 100 \cdot f_1 \cdot f_2 \cdot f_3 & \sigma_s &= \frac{1}{100} \\ \rho(\mathbf{x} \in \Gamma_I) &= 0 & \rho(\mathbf{x} \in \Gamma_{II}) &= \frac{1}{2} & \rho(\mathbf{x} \in \Gamma_{III}) &= 0 & \rho(\mathbf{x} \in \Gamma_{IV}) &= \frac{1}{2} \\ I_\Gamma(\mathbf{x} \in \Gamma_I, \mathbf{\Omega}) &= 0 & I_\Gamma(\mathbf{x} \in \Gamma_{II}, \mathbf{\Omega}) &= 0 & I_\Gamma(\mathbf{x} \in \Gamma_{III}, \mathbf{\Omega}) &= \frac{1}{4\pi} & I_\Gamma(\mathbf{x} \in \Gamma_{IV}, \mathbf{\Omega}) &= 0 \end{aligned}$$

Table 9: Setup for test case 4

For the spatial discretization we use a triangular mesh with 2699 nodes and 5252 elements. We refine the mesh by splitting [78] and obtain a mesh with 10649 nodes and 21008 elements for numerical reference solutions of the corresponding models, denoted by $P_N^{2nd, \text{fine}}$. As reference we compute the discrete ordinates solution on the coarse mesh. As before we use for the discretization of the unit sphere a Gaussian-like quadrature rule which is exact for polynomials up to degree 23 and leaves us with 600 ordinates on the upper half sphere after reduction to 2D. We compare this solution to the discrete ordinates solution with a quadrature rule exact up to degree 15 with 272 ordinates on the upper half sphere.

In Figure 5 we show the radiative energies of the discrete ordinates solution and the $P_1^{2nd}, P_3^{2nd}, P_5^{2nd}$ solutions. In Table 11 we show the relative L^2 distances of the radiative energies of the P_N^{2nd} solutions on the

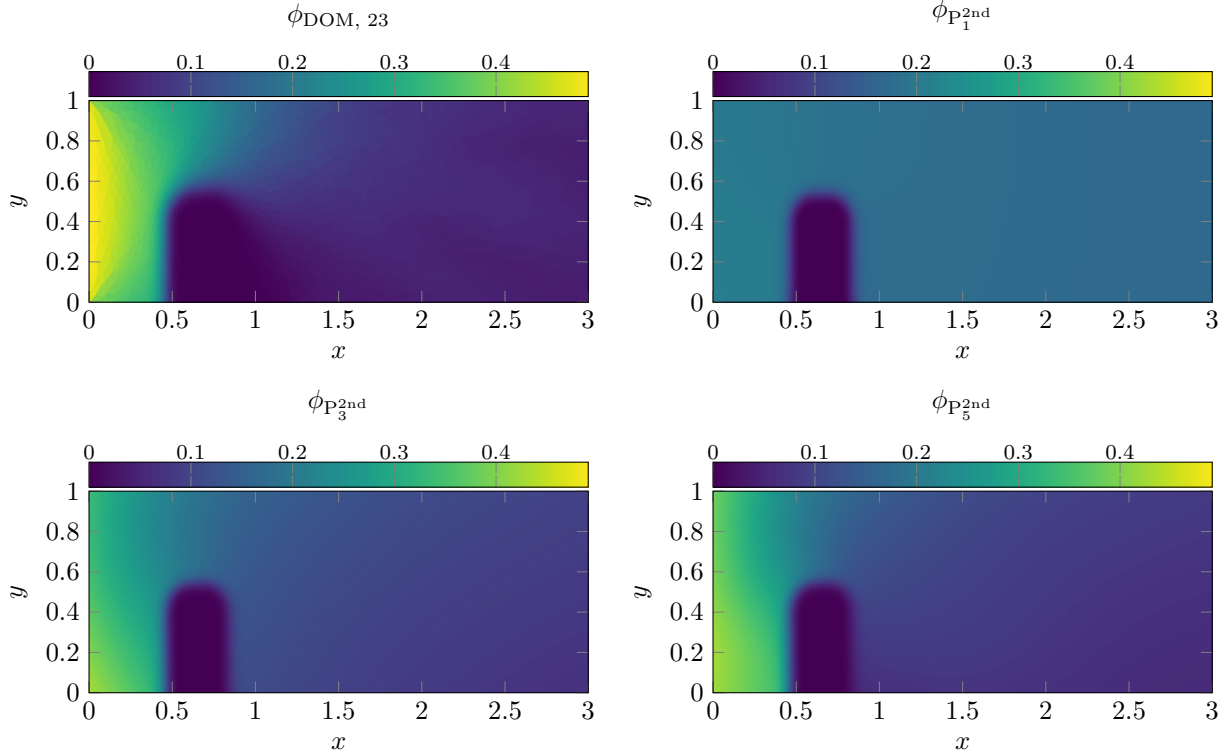


Figure 5: Test case 4

coarse grid to the corresponding reference solutions on the refined grid and the discrete ordinates solution.

We see that the distance of the radiative energies of the P_N^{2nd} solutions to the discrete ordinates solutions decreases, but it seems that a much larger moment order N would be necessary to get a satisfying approximation. Furthermore we would like to note that the presented discrete ordinates solution is only to a certain extent suitable as a reference solution, as its relative L^2 distance to the solution with around half as many discrete ordinates is about 4%.

Referring to our repository on GitHub [22], we list the functions used to compute the different approximations of the distribution and radiative energy in Table 10.

wrapper		<code>runTestCase4.m</code>
mesh generation and refinement		<code>genMeshTestCase4.sh</code>
discrete ordinates method	ϕ_{DOM}	<code>runDiscreteOrdinatesTestCase4.m</code>
P_N^{2nd} solution	$\phi_{P_N^{2nd}}$	<code>runTestCase4.py</code>
transformation $P_N \rightarrow P_N^{2nd}$		<code>generateTestCase4.m</code>

Table 10: Implementation of test case 4

4.6. Test case 5

The fifth test case considers the popular Henyey Greenstein scattering kernel. This especially demonstrates that our method is not limited to isotropic scattering. For the spatial discretization we use a triangular mesh with 2212 nodes and 4262 elements. We refine the mesh by splitting [78] and obtain a mesh with 8685 nodes and 17048 elements for numerical reference solutions of the corresponding models, denoted by $P_N^{2nd, fine}$. As reference we compute the discrete ordinates solution on the coarse mesh. As before we use for the discretization of the unit sphere a Gaussian-like quadrature rule which is exact for polynomials up to

N	$\frac{\ \phi_{P_N^{2nd}} - \phi_{P_N^{2nd, fine}}\ _{L^2(X)}}{\ \phi_{P_N^{2nd, fine}}\ _{L^2(X)}}$	$\frac{\ \phi - \phi_{DOM, 23}\ _{L^2(X)}}{\ \phi_{DOM, 23}\ _{L^2(X)}}$
1	2.03e-03	7.18e-01
3	2.39e-03	3.41e-01
5	1.01e-02	2.47e-01
7	1.40e-02	1.91e-01

Table 11: Relative differences test case 4, with $\frac{\|\phi_{DOM, 15} - \phi_{DOM, 23}\|_{L^2(X)}}{\|\phi_{DOM, 23}\|_{L^2(X)}} = 3.61e-02$

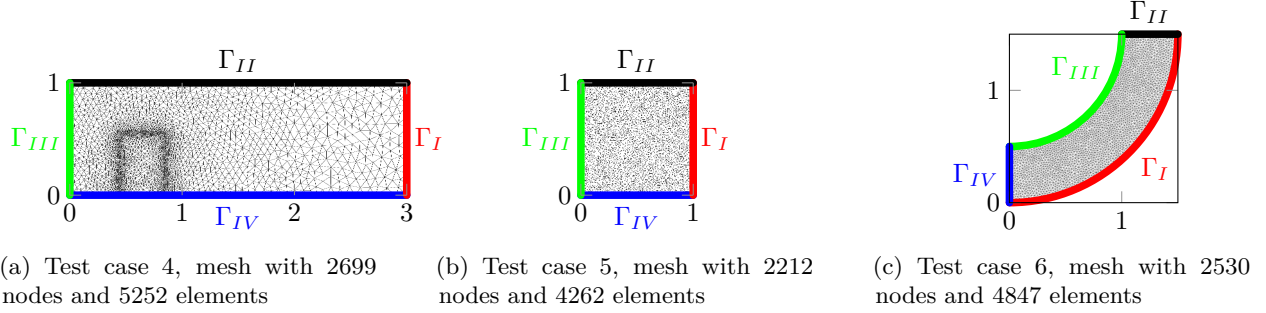


Figure 6: Meshes and boundary conditions

degree 23 and leaves us with 600 ordinates on the full unit sphere. We compare this solution to the discrete ordinates solution with a quadrature rule exact up to degree 15 with 272 ordinates on the full unit sphere.

The setup for this test case in 2D is given in Table 12. The domain X and the partition of the boundary $\Gamma = \Gamma_I \cup \Gamma_{II} \cup \Gamma_{III} \cup \Gamma_{IV}$ are illustrated in Figure 6b. We choose the anisotropy factor in the Henyey-Greenstein kernel $g = 0.5$.

$$\begin{array}{llll}
X = [0, 1]^2 & \kappa(\mathbf{\Omega}, \mathbf{\Omega}') = \frac{1}{4\pi} \frac{1-g^2}{(1+g^2-2g \cos(\mathbf{\Omega}^T \mathbf{\Omega}'))^{3/2}} & \sigma_a = 0 & \sigma_s = 1 \\
\rho(\mathbf{x} \in \Gamma_I) = 0 & \rho(\mathbf{x} \in \Gamma_{II}) = 0.99 & \rho(\mathbf{x} \in \Gamma_{III}) = 0 & \rho(\mathbf{x} \in \Gamma_{IV}) = 0.99 \\
I_\Gamma(\mathbf{x} \in \Gamma_I, \mathbf{\Omega}) = 0 & I_\Gamma(\mathbf{x} \in \Gamma_{II}, \mathbf{\Omega}) = 0 & I_\Gamma(\mathbf{x} \in \Gamma_{III}, \mathbf{\Omega}) = \mathbf{\Omega}_x & I_\Gamma(\mathbf{x} \in \Gamma_{IV}, \mathbf{\Omega}) = 0
\end{array}$$

Table 12: Setup for test case 5

In Figure 7 we show the radiative energies of the discrete ordinates solution and the $P_1^{2nd}, P_3^{2nd}, P_5^{2nd}$ solutions. In Figure 8 we compare the radiative energies for different model orders and the anisotropy factors $g = 0$ and $g = 0.5$ along the line $\{(x, y) \in X : y = 0.5\}$. We would like to note, that $g = 0$ reproduces anisotropic scattering. The non-smoothness in the line plot of the discrete ordinates solution is caused by interpolation of the corresponding piecewise constant function w.r.t. the elements. In Table 14 we show the relative L^2 distances of the radiative energies of the P_N^{2nd} solutions on the coarse grid to the corresponding reference solutions on the refined grid and the discrete ordinates solution.

Referring to our repository on GitHub [22], we list the functions used to compute the different approximations of the distribution and radiative energy in Table 13.

4.7. Test case 6

This test case demonstrates that our method is not limited to rectangular domains and especially can be used with irregular grids.

For the spatial discretization we use a triangular mesh with 2530 nodes and 4847 elements. We refine the mesh by splitting [78] and obtain a mesh with 9906 nodes and 19388 elements for numerical reference solutions

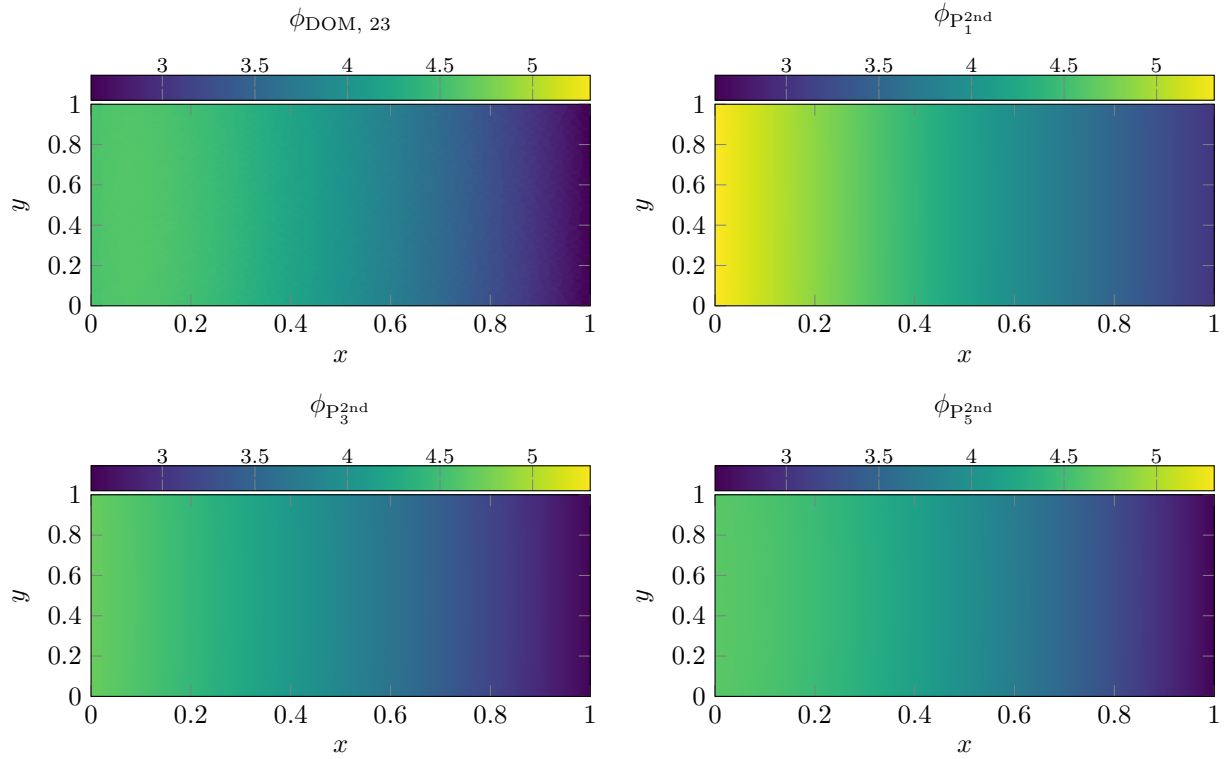


Figure 7: Test case 5

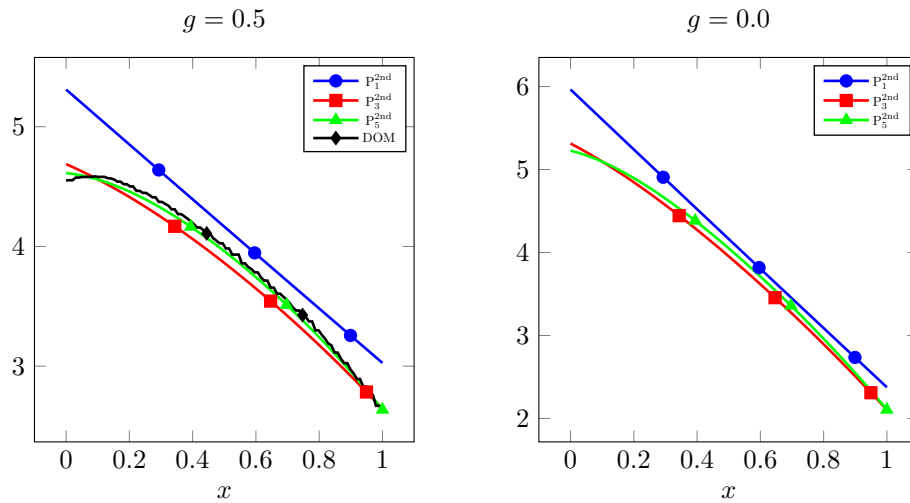


Figure 8: Test case 5: Radiative energies along $\{(x, y) \in X : y = 0.5\}$

wrapper		<code>runTestCase5.m</code>
mesh generation and refinement		<code>genMeshTestCase5.sh</code>
discrete ordinates method	ϕ_{DOM}	<code>runDiscreteOrdinatesTestCase5.m</code>
$P_N^{2\text{nd}}$ solution	$\phi_{P_N^{2\text{nd}}}$	<code>runTestCase5.py</code>
transformation $P_N \rightarrow P_N^{2\text{nd}}$		<code>generateTestCase5.m</code>

Table 13: Implementation of test case 5

N	$\frac{\ \phi_{P_N^{2\text{nd}}} - \phi_{P_N^{2\text{nd},\text{fine}}}\ _{L^2(X)}}{\ \phi_{P_N^{2\text{nd},\text{fine}}}\ _{L^2(X)}}$	$\frac{\ \phi_{P_N^{2\text{nd}}} - \phi_{\text{DOM}, 23}\ _{L^2(X)}}{\ \phi_{\text{DOM}, 23}\ _{L^2(X)}}$
1	3.55e-07	8.07e-02
3	1.75e-05	2.73e-02
5	4.12e-05	1.02e-02
7	7.26e-05	4.03e-03

Table 14: Relative differences test case 5, with $\frac{\|\phi_{\text{DOM}, 15} - \phi_{\text{DOM}, 23}\|_{L^2(X)}}{\|\phi_{\text{DOM}, 23}\|_{L^2(X)}} = 4.75\text{e-}03$

of the corresponding models, denoted by $P_N^{2\text{nd},\text{fine}}$. As reference we compute the discrete ordinates solution on the coarse mesh. As before we use for the discretization of the unit sphere a Gaussian-like quadrature rule which is exact for polynomials up to degree 23 and leaves us with 600 ordinates on the upper half sphere. We compare this solution to the discrete ordinates solution with a quadrature rule exact up to degree 15 with 272 ordinates on the upper half sphere.

The setup for this test case in 2D is given in Table 15. The domain X and the partition of the boundary $\Gamma = \Gamma_I \cup \Gamma_{II} \cup \Gamma_{III} \cup \Gamma_{IV}$ is illustrated in Figure 6c.

$$\begin{aligned}
X: \text{ see Figure 6c} \quad \kappa(\mathbf{\Omega}, \mathbf{\Omega}') &= \frac{1}{4\pi} & \sigma_a &= 0 & \sigma_s &= \frac{1}{10} \\
\rho(\mathbf{x} \in \Gamma_I) &= 0.5 & \rho(\mathbf{x} \in \Gamma_{II}) &= 0 & \rho(\mathbf{x} \in \Gamma_{III}) &= 0.5 & \rho(\mathbf{x} \in \Gamma_{IV}) &= 0 \\
I_\Gamma(\mathbf{x} \in \Gamma_I) &= 0 & I_\Gamma(\mathbf{x} \in \Gamma_{II}) &= 0 & I_\Gamma(\mathbf{x} \in \Gamma_{III}) &= 0 & I_\Gamma(\mathbf{x} \in \Gamma_{IV}) &= 1
\end{aligned}$$

Table 15: Setup for test case 6

In Figure 9 we show the radiative energies of the discrete ordinates solution and the $P_1^{2\text{nd}}, P_3^{2\text{nd}}, P_5^{2\text{nd}}$ solutions. In Table 17 we show the relative L^2 distances of the radiative energies of the $P_N^{2\text{nd}}$ solutions on the coarse grid to the corresponding reference solutions on the refined grid and the discrete ordinates solution.

Referring to our repository on GitHub [22], we list the functions used to compute the different approximations of the distribution and radiative energy in Table 16.

wrapper		<code>runTestCase6.m</code>
mesh generation and refinement		<code>genMeshTestCase6.sh</code>
discrete ordinates method	ϕ_{DOM}	<code>runDiscreteOrdinatesTestCase6.m</code>
$P_N^{2\text{nd}}$ solution	$\phi_{P_N^{2\text{nd}}}$	<code>runTestCase6.py</code>
transformation $P_N \rightarrow P_N^{2\text{nd}}$		<code>generateTestCase6.m</code>

Table 16: Implementation of test case 6

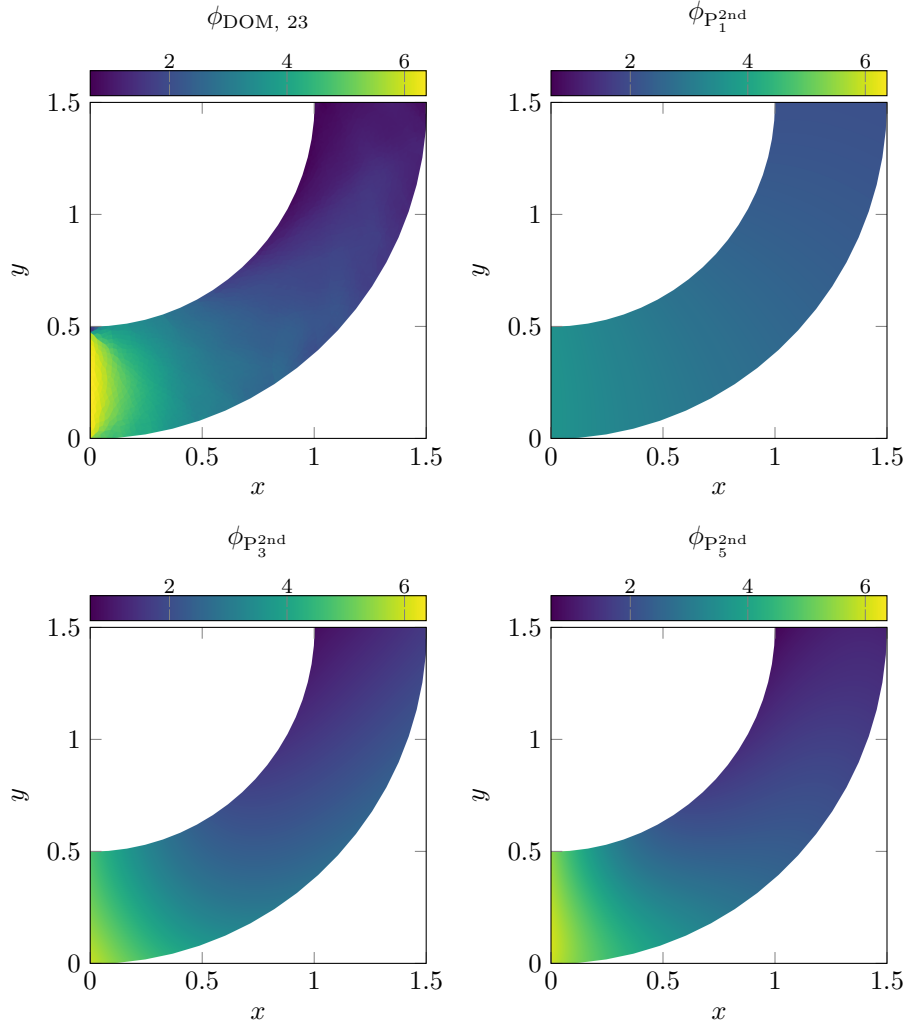


Figure 9: Test case 6

N	$\frac{\ \phi_{P_N^{2nd}} - \phi_{P_N^{2nd}, \text{fine}}\ _{L^2(X)}}{\ \phi_{P_N^{2nd}, \text{fine}}\ _{L^2(X)}}$	$\frac{\ \phi_{P_N^{2nd}} - \phi_{\text{DOM}, 23}\ _{L^2(X)}}{\ \phi_{\text{DOM}, 23}\ _{L^2(X)}}$
1	1.00e-05	3.34e-01
3	3.77e-04	1.43e-01
5	1.08e-03	9.53e-02
7	4.00e-03	8.48e-02

Table 17: Relative differences test case 6, with $\frac{\|\phi_{\text{DOM}, 15} - \phi_{\text{DOM}, 23}\|_{L^2(X)}}{\|\phi_{\text{DOM}, 23}\|_{L^2(X)}} = 3.54\text{e-}02$

5. Conclusion

We presented the second-order formulation of the classical P_N equations for the monoenergetic stationary linear transport equation. In contrary to classical SP_N approaches, we reproduce the even moments of the original P_N system.

We approximate the semi-transparent boundary conditions on the kinetic level by taking half moments at the boundary and obtain Marshak boundary conditions. Taking half moments at the boundary w.r.t. all real spherical harmonics up to the used order N would yield too many boundary conditions, where our derivation suggests the “natural” selection of a subset of those real spherical harmonics based on the weak formulation.

The algebraic transformations can be handed to a computer algebra system and the solution of the resulting weak formulation can be delegated to established PDE tools. We demonstrated this workflow with MATLAB’s symbolic toolbox and FEniCS. Our implementation is not necessarily designed to yield a high performance solution scheme, in fact it should be seen as a proof of concept and easy-to-use tool for fast prototyping.

We demonstrated in six numerical test cases the flexibility and wide applicability of our approach.

Our derivation is based on the assumption, that all algebraic elimination steps are justified. Especially we assume that the solution of the original P_N system is of certain regularity and that all (higher order) derivatives are well defined. We proved, under these regularity assumptions on the P_N solutions and mild additional assumptions in Lemmas 3.5, 3.6 and 3.7, that the resulting second-order formulation is well defined. It would be an interesting task for the future to investigate the well-posedness of the resulting system.

Acknowledgement

The authors are grateful for the support of the German Federal Ministry of Education and Research (BMBF) grant no. 05M16UKE.

References

- [1] F. Hübner, C. Leithäuser, B. Bazrafshan, N. Siedow, T. J. Vogl, [Validation of a mathematical model for laser-induced thermotherapy in liver tissue](#), *Lasers in Medical Science* 32 (6) (2017) 1399–1409. doi:10.1007/s10103-017-2260-4. URL <https://doi.org/10.1007/s10103-017-2260-4>
- [2] R. Pinnau, G. Thömmes, Optimal boundary control of glass cooling processes, *Mathematical methods in the applied sciences* 27 (11) (2004) 1261–1281.
- [3] T. A. Brunner, Forms of approximate radiation transport, Sandia report.
- [4] B. Seibold, M. Frank, [Starmap—a second order staggered grid method for spherical harmonics moment equations of radiative transfer](#), *ACM Transactions on Mathematical Software* 41 (1) (2014) 4:1–4:28. doi:10.1145/2590808. URL <http://doi.acm.org/10.1145/2590808>
- [5] W. Ge, R. Marquez, M. F. Modest, S. P. Roy, Implementation of high-order spherical harmonics methods for radiative heat transfer on openfoam, *Journal of Heat Transfer* 137 (5) (2015) 052701.
- [6] J. T. Tencer, [Error analysis for radiation transport](#), dissertation, The University of Texas at Austin (2013). URL <https://repositories.lib.utexas.edu/handle/2152/23247>
- [7] R. G. McClarren, [Theoretical aspects of the simplified \$P_n\$ equations](#), *Transport Theory and Statistical Physics* 39 (2-4) (2010) 73–109. doi:10.1080/00411450.2010.535088. URL <https://doi.org/10.1080/00411450.2010.535088>

- [8] M. F. Modest, J. Yang, [Elliptic pde formulation and boundary conditions of the spherical harmonics method of arbitrary order for general three-dimensional geometries](#), Journal of Quantitative Spectroscopy and Radiative Transfer 109 (9) (2008) 1641 – 1666. doi:<https://doi.org/10.1016/j.jqsrt.2007.12.018>.
URL <http://www.sciencedirect.com/science/article/pii/S0022407307003676>
- [9] M. F. Modest, [Further development of the elliptic pde formulation of the p_n approximation and its marshak boundary conditions](#), Numerical Heat Transfer, Part B: Fundamentals 62 (2-3) (2012) 181–202. doi:[10.1080/10407790.2012.702645](https://doi.org/10.1080/10407790.2012.702645).
URL <https://doi.org/10.1080/10407790.2012.702645>
- [10] W. Ge, High-order spherical harmonics methods for radiative heat transfer and applications in combustion simulations, Ph.D. thesis, UC Merced (2017).
- [11] A. D. Kloze, E. W. Larsen, [Light transport in biological tissue based on the simplified spherical harmonics equations](#), Journal of Computational Physics 220 (1) (2006) 441 – 470. doi:<https://doi.org/10.1016/j.jcp.2006.07.007>.
URL <http://www.sciencedirect.com/science/article/pii/S0021999106003421>
- [12] S. P. Hamilton, T. M. Evans, [Efficient solution of the simplified \$P_N\$ equations](#), Journal of Computational Physics 284 (2015) 155 – 170. doi:<https://doi.org/10.1016/j.jcp.2014.12.014>.
URL <http://www.sciencedirect.com/science/article/pii/S0021999114008225>
- [13] M. F. Modest, J. Cai, W. Ge, E. Lee, [Elliptic formulation of the simplified spherical harmonics method in radiative heat transfer](#), International Journal of Heat and Mass Transfer 76 (2014) 459 – 466. doi:<https://doi.org/10.1016/j.ijheatmasstransfer.2014.04.038>.
URL <http://www.sciencedirect.com/science/article/pii/S0017931014003433>
- [14] Y. Zhang, J. C. Ragusa, J. E. Morel, [Iterative performance of various formulations of the \$sP_N\$ equations](#), Journal of Computational Physics 252 (2013) 558 – 572. doi:<https://doi.org/10.1016/j.jcp.2013.06.009>.
URL <http://www.sciencedirect.com/science/article/pii/S0021999113004336>
- [15] K. Liu, Y. Lu, J. Tian, C. Qin, X. Yang, S. Zhu, X. Yang, Q. Gao, D. Han, [Evaluation of the simplified spherical harmonics approximation in bioluminescence tomography through heterogeneous mouse models](#), Opt. Express 18 (20) (2010) 20988–21002. doi:[10.1364/OE.18.020988](https://doi.org/10.1364/OE.18.020988).
URL <http://www.opticsexpress.org/abstract.cfm?URI=oe-18-20-20988>
- [16] C. Pu, R. G. McClarren, [Mathematical and numerical validation of the simplified spherical harmonics approach for time-dependent anisotropic-scattering transport problems in homogeneous media](#), Journal of Computational and Theoretical Transport 46 (5) (2017) 366–378. doi:[10.1080/23324309.2017.1352516](https://doi.org/10.1080/23324309.2017.1352516).
URL <https://doi.org/10.1080/23324309.2017.1352516>
- [17] MATLAB, [Matlab and symbolic toolbox release 2018b](#) (2018).
URL <https://de.mathworks.com/>
- [18] M. Alnæs, J. Blechta, J. Hake, A. Johansson, B. Kehlet, A. Logg, C. Richardson, J. Ring, M. E. Rognes, G. N. Wells, [The fenics project version 1.5](#), Archive of Numerical Software 3 (100) (2015) 9–23.
URL <https://fenicsproject.org/>
- [19] A. Logg, K.-A. Mardal, G. Wells, Automated Solution of Differential Equations by the Finite Element Method: The FEniCS Book, Vol. 84, Springer Science & Business Media, 2012.
- [20] R. J. LeVeque, Python tools for reproducible research on hyperbolic problems, Computing in Science Engineering 11 (1) (2009) 19–27. doi:[10.1109/MCSE.2009.13](https://doi.org/10.1109/MCSE.2009.13).

- [21] M. D. Wilkinson, M. Dumontier, I. J. Aalbersberg, G. Appleton, M. Axton, A. Baak, N. Blomberg, J.-W. Boiten, L. B. da Silva Santos, P. E. Bourne, et al., The fair guiding principles for scientific data management and stewardship, *Scientific data* 3.
- [22] M. Andres, F. Schneider, Github repository for this project, <https://github.com/andresmatthias/pn2nd.git>, contains MATLAB and Python codes related to this article to reproduce the numerical results. Accessed: 2019-08-01.
- [23] C. Cercignani, [The Boltzmann Equation and its Applications](#), Applied mathematical sciences ; 67, Springer, Berlin u.a., 1988.
URL <https://kplus.ub.uni-kl.de/Record/KLU01-000183612>
- [24] S. J. Park, S.-B. Yun, [Entropy production estimates for the polyatomic ellipsoidal bgk model](#), Applied Mathematics Letters 58 (2016) 26 – 33. doi:<https://doi.org/10.1016/j.aml.2016.01.021>.
URL <http://www.sciencedirect.com/science/article/pii/S089396591630043X>
- [25] C. D. Levermore, [Moment closure hierarchies for kinetic theories](#), Journal of Statistical Physics 83 (5) (1996) 1021–1065. doi:[10.1007/BF02179552](https://doi.org/10.1007/BF02179552).
URL <https://doi.org/10.1007/BF02179552>
- [26] L. G. Henyey, J. L. Greenstein, Diffuse radiation in the galaxy, *Astrophysical Journal* 93 (1941) 70–83. doi:[10.1086/144246](https://doi.org/10.1086/144246).
- [27] E. W. Larsen, G. Thömmes, A. Klar, M. Seaïd, T. Götz, [Simplified \$P_N\$ approximations to the equations of radiative heat transfer and applications](#), Journal of Computational Physics 183 (2) (2002) 652 – 675. doi:<https://doi.org/10.1006/jcph.2002.7210>.
URL <http://www.sciencedirect.com/science/article/pii/S0021999102972104>
- [28] E. Olbrant, M. Frank, [Generalized fokker-planck theory for electron and photon transport in biological tissues: Application to radiotherapy](#), Computational and mathematical methods in medicine 11 (4) (2010) 313–39. doi:[10.1080/1748670X.2010.491828](https://doi.org/10.1080/1748670X.2010.491828).
URL <http://www.ncbi.nlm.nih.gov/pubmed/20924856>
- [29] B. Dubroca, J.-L. Feugeas, M. Frank, [Angular moment model for the fokker-planck equation](#), The European Physical Journal D 60 (2) (2010) 301–307. doi:[10.1140/epjd/e2010-00190-8](https://doi.org/10.1140/epjd/e2010-00190-8).
URL <http://www.springerlink.com/index/10.1140/epjd/e2010-00190-8>
- [30] F. Schneider, [Moment models in radiation transport equations](#), Ph.D. thesis, TU Kaiserslautern, München (2016).
URL <https://kplus.ub.uni-kl.de/Record/KLU01-001010407>
- [31] T. A. Brunner, J. P. Holloway, [Two-dimensional time dependent riemann solvers for neutron transport](#), Journal of Computational Physics 210 (1) (2005) 386 – 399. doi:<https://doi.org/10.1016/j.jcp.2005.04.011>.
URL <http://www.sciencedirect.com/science/article/pii/S0021999105002275>
- [32] M. A. Blanco, M. Flórez, M. Bermejo, [Evaluation of the rotation matrices in the basis of real spherical harmonics](#), Journal of Molecular Structure: THEOCHEM 419 (1) (1997) 19 – 27. doi:[https://doi.org/10.1016/S0166-1280\(97\)00185-1](https://doi.org/10.1016/S0166-1280(97)00185-1).
URL <http://www.sciencedirect.com/science/article/pii/S0166128097001851>
- [33] R. Courant, D. Hilbert, [Methods of Mathematical Physics](#), no. Bd. 1 in *Methods of Mathematical Physics*, Wiley, 2008.
URL <https://archive.org/details/MethodsOfMathematicalPhysicsVolume1>
- [34] A. S. Eddington, *The Internal Constitution of the Stars*, Dover, 1926.

- [35] E. E. Lewis, J. W. F. Miller, *Computational Methods in Neutron Transport*, John Wiley and Sons, New York, 1984.
- [36] E. Tadmor, *Approximate Solutions of Nonlinear Conservation Laws*, Springer, 1998.
URL <http://link.springer.com/chapter/10.1007/BFb0096352>
- [37] C.-W. Shu, *Essentially Non-Oscillatory and Weighted Essentially Non-Oscillatory Schemes for Hyperbolic Conservation Laws*, Springer, 1998.
URL <http://link.springer.com/chapter/10.1007/BFb0096355>
- [38] C. K. Garrett, C. D. Hauck, *A comparison of moment closures for linear kinetic transport equations: The line source benchmark*, *Transport Theory and Statistical Physics*.
URL <http://www.tandfonline.com/doi/abs/10.1080/00411450.2014.910226>
- [39] P. Chidyagwai, M. Frank, F. Schneider, B. Seibold, *A comparative study of limiting strategies in discontinuous galerkin schemes for the m1 model of radiation transport*, *Journal of Computational and Applied Mathematics* 342 (2018) 399 – 418. doi:<https://doi.org/10.1016/j.cam.2018.04.017>.
URL <http://www.sciencedirect.com/science/article/pii/S0377042718301857>
- [40] C. D. Levermore, *Relating eddington factors to flux limiters*, *Journal of Quantitative Spectroscopy and Radiative ...* 31 (2) (1984) 149–160.
URL <http://www.sciencedirect.com/science/article/pii/0022407384901122>
- [41] L. R. Mead, N. Papanicolaou, *Maximum entropy in the problem of moments*, *Journal of Mathematical Physics* 25 (8) (1984) 2404. doi:[10.1063/1.526446](https://doi.org/10.1063/1.526446).
URL <http://link.aip.org/link/JMAPAQ/v25/i8/p2404/s1{&}Agg=doi>
- [42] J. Cernohorsky, S. Bludman, *Maximum entropy distribution and closure for bose-einstein and fermi-dirac radiation transport*, *The Astrophysical Journal*.
URL <http://adsabs.harvard.edu/full/1994ApJ...433..250C>
- [43] B. Dubroca, J.-L. Feugeas, *Entropic moment closure hierarchy for the radiative transfer equation*, *C. R. Acad. Sci. Paris Ser. I* 329 (1999) 915–920.
- [44] M. Junk, *Maximum entropy for reduced moment problems*, *Math. Meth. Mod. Appl. Sci.* 10 (2000) 1001–1025.
- [45] G. N. Minerbo, *Maximum entropy eddington factors*, *J. Quant. Spectrosc. Radiat. Transfer* 20 (1978) 541–545.
- [46] T. A. Brunner, J. P. Holloway, *One-dimensional riemann solvers and the maximum entropy closure*, *Journal of Quantitative Spectroscopy and Radiative Transfer* 69 (5) (2001) 543–566. doi:[10.1016/S0022-4073\(00\)00099-6](https://doi.org/10.1016/S0022-4073(00)00099-6).
URL <http://www.sciencedirect.com/science/article/pii/S0022407300000996>
<http://linkinghub.elsevier.com/retrieve/pii/S0022407300000996>
- [47] E. Olbrant, C. D. Hauck, M. Frank, *A realizability-preserving discontinuous galerkin method for the m1 model of radiative transfer*, *Journal of Computational Physics* 231 (17) (2012) 5612–5639. doi:[10.1016/j.jcp.2012.03.002](https://doi.org/10.1016/j.jcp.2012.03.002).
URL <http://linkinghub.elsevier.com/retrieve/pii/S0021999112001362>
- [48] C. D. Hauck, *High-order entropy-based closures for linear transport in slab geometry*, *Commun. Math. Sci.* v9.
URL http://www.ki-net.umd.edu/pubs/files/FRG-2010-Hauck-Cory_entropy_{ }kinetic.pdf
- [49] G. W. Alldredge, C. D. Hauck, A. L. Tits, *High-order entropy-based closures for linear transport in slab geometry ii: A computational study of the optimization problem*, *SIAM Journal on Scientific Computing* 34 (4) (2012) B361–B391. doi:[10.1137/11084772X](https://doi.org/10.1137/11084772X).
URL <http://epubs.siam.org/doi/abs/10.1137/11084772X>

- [50] F. Schneider, T. Leibner, First-order continuous- and discontinuous-galerkin moment models for a linear kinetic equation: Realizability-preserving splitting scheme and numerical analysis (2019). [arXiv:1904.03098](#).
- [51] M. Frank, B. Dubroca, A. Klar, [Partial moment entropy approximation to radiative heat transfer](#), Journal of Computational Physics 218 (1) (2006) 1–18.
URL <http://www.sciencedirect.com/science/article/pii/S002199910600057X>
- [52] B. Dubroca, A. Klar, [Half-moment closure for radiative transfer equations](#), Journal of Computational Physics 180 (2002) 584–596.
URL <http://www.sciencedirect.com/science/article/pii/S0021999102971068>
- [53] F. Schneider, G. W. Alldredge, M. Frank, A. Klar, [Higher order mixed-moment approximations for the fokker–planck equation in one space dimension](#), SIAM Journal on Applied Mathematics 74 (4) (2014) 1087–1114. [arXiv:1405.5305](#), [doi:10.1137/130934210](#).
URL <http://epubs.siam.org/doi/abs/10.1137/130934210>
- [54] J. Ritter, A. Klar, F. Schneider, [Partial-moment minimum-entropy models for kinetic chemotaxis equations in one and two dimensions](#), Journal of Computational and Applied Mathematics 306 (2016) 300–315. [arXiv:1601.04482](#), [doi:10.1016/j.cam.2016.04.019](#).
URL <http://arxiv.org/abs/1601.04482>
- [55] F. Schneider, J. Kall, A. Roth, [First-order quarter- and mixed-moment realizability theory and kershaw closures for a fokker-planck equation in two space dimensions](#), Kinetic and Related Models 10. [doi:10.3934/krm.2017044](#).
URL <http://aims sciences.org//article/id/92206f8c-b216-478b-a566-d72a803c8ab9>
- [56] D. S. Kershaw, [Flux limiting nature’s own way: A new method for numerical solution of the transport equation](#), Tech. rep., LLNL Report UCRL-78378 (jul 1976). [doi:10.2172/104974](#).
URL http://www.osti.gov/bridge/product.biblio.jsp?osti_{_}id=104974
- [57] P. Monreal, Moment realizability and kershaw closures in radiative transfer, Ph.D. thesis, TU Aachen (2012).
- [58] F. Schneider, [Kershaw closures for linear transport equations in slab geometry i: Model derivation](#), Journal of Computational Physics 322 (2016) 905–919. [arXiv:1511.02714](#), [doi:10.1016/j.jcp.2016.02.080](#).
URL <http://arxiv.org/abs/1511.02714>
- [59] F. Schneider, [Kershaw closures for linear transport equations in slab geometry ii: high-order realizability-preserving discontinuous-galerkin schemes](#), Journal of Computational Physics 322 (2016) 920–935. [arXiv:1602.02590](#), [doi:10.1016/j.jcp.2016.07.014](#).
URL <http://arxiv.org/abs/1602.02590>
- [60] E. d’Eon, [A hitchhiker’s guide to multiple scattering](#), Tech. rep., Technical report (2016).
URL <http://www.eugenedeon.com/hitchhikers>
- [61] S. Chandrasekhar, Radiative Transfer, Courier Corporation, 2013.
- [62] H. Kagiwada, R. Kalaba, Multiple anisotropic scattering in slabs with axially symmetric fields, Tech. rep., RAND CORP SANTA MONICA CALIF (1967).
- [63] I. Gkioulekas, B. Xiao, S. Zhao, E. H. Adelson, T. Zickler, K. Bala, [Understanding the role of phase function in translucent appearance](#), ACM Trans. Graph. 32 (5) (2013) 147:1–147:19. [doi:10.1145/2516971.2516972](#).
URL <http://doi.acm.org/10.1145/2516971.2516972>

- [64] E. F. Toro, [Riemann Solvers and Numerical Methods for Fluid Dynamics](#), 3rd Edition, Springer, Dordrecht u.a., 2009.
URL <https://kplus.ub.uni-kl.de/Record/KLU01-000747419>
- [65] G. C. Pomraning, [Variational boundary conditions for the spherical harmonics approximation to the neutron transport equation](#), *Annals of Physics* 27 (2) (1964) 193 – 215. doi:[https://doi.org/10.1016/0003-4916\(64\)90105-8](https://doi.org/10.1016/0003-4916(64)90105-8).
URL <http://www.sciencedirect.com/science/article/pii/0003491664901058>
- [66] E. W. Larsen, G. C. Pomraning, [The PN Theory as an Asymptotic Limit of Transport Theory in Planar Geometry —I: Analysis](#), *Nuclear Science and Engineering* 109 (1) (1991) 49–75.
URL <http://epubs.ans.org/?a=23844>
- [67] R. P. Rulko, E. W. Larsen, G. C. Pomraning, [The PN Theory as an Asymptotic Limit of Transport Theory in Planar Geometry —II: Numerical Results](#), *Nuclear Science and Engineering* 109 (1) (1991) 76–85.
URL <http://epubs.ans.org/?a=23845>
- [68] H. Struchtrup, [Kinetic schemes and boundary conditions for moment equations](#), *Zeitschrift für angewandte Mathematik und Physik* 51 (3) (2000) 346. doi:[10.1007/s000330050002](https://doi.org/10.1007/s000330050002).
URL <http://link.springer.com/10.1007/s000330050002>
- [69] C. D. Levermore, [Boundary conditions for moment closures](#), Institute for Pure and Applied Mathematics University of California, Los Angeles, CA on May 27.
- [70] S. P. Hamilton, T. M. Evans, [Efficient solution of the simplified pn equations](#), *Journal of Computational Physics* 284 (2015) 155 – 170. doi:<https://doi.org/10.1016/j.jcp.2014.12.014>.
URL <http://www.sciencedirect.com/science/article/pii/S0021999114008225>
- [71] G. Da Fies, M. Vianello, [Trigonometric gaussian quadrature on subintervals of the period](#), *Electronic Transactions on Numerical Analysis* 39 (2012) 102–112.
- [72] G. Da Fies, A. Sommariva, V. M., [Subp: Matlab package for subperiodic trigonometric quadrature and multivariate applications](#), <https://www.math.unipd.it/~marcov/mysoft/subp/trigauss.m>, contains codes for product Gaussian quadrature on circular and spherical sections.
- [73] E. W. Larsen, J. E. Morel, [Advances in discrete-ordinates methodology](#), in: *Nuclear Computational Science*, Springer, 2010, pp. 1–84.
- [74] M. F. Carfora, [Interpolation on spherical geodesic grids: A comparative study](#), *Journal of Computational and Applied Mathematics* 210 (1) (2007) 99 – 105, proceedings of the Numerical Analysis Conference 2005. doi:<https://doi.org/10.1016/j.cam.2006.10.068>.
URL <http://www.sciencedirect.com/science/article/pii/S0377042706006522>
- [75] T. P. S. Foundation, [Python](#).
URL <https://www.python.org/>
- [76] T. E. Oliphant, [A Guide to NumPy](#), Vol. 1, Trelgol Publishing USA, 2006.
URL <https://numpy.org/>
- [77] E. Jones, T. Oliphant, P. Peterson, et al., [SciPy: Open source scientific tools for Python](#) (2001–).
URL <http://www.scipy.org/>
- [78] C. Geuzaine, J.-F. Remacle, [Gmsh: a three-dimensional finite element mesh generator with built-in pre- and post-processing facilities](#), *International Journal for Numerical Methods in Engineering* 79 (2009) 1309–1331.
URL <http://www.gmsh.info/>